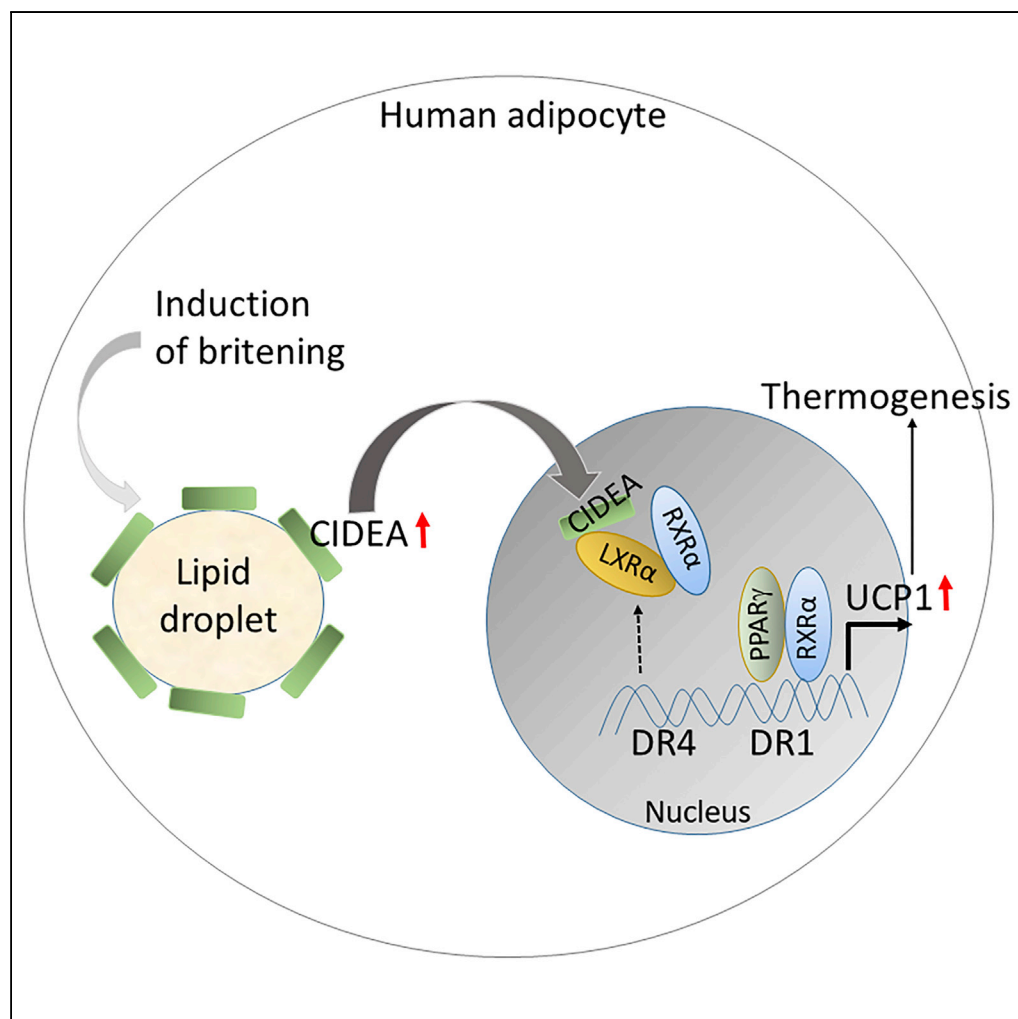


## Article

## CIDEA Transcriptionally Regulates UCP1 for Britening and Thermogenesis in Human Fat Cells



Sukanta Jash,  
Sayani Banerjee,  
Mi-Jeong Lee,  
Stephen R.  
Farmer,  
Vishwajeet Puri

puri@ohio.edu

## HIGHLIGHTS

CIDEA knockout inhibits  
britening and uncoupling  
in human adipocytes

The induction of britening  
induces CIDEA expression  
and nuclear translocation

CIDEA inhibits LXR $\alpha$   
repression of UCP1  
enhancer activity

CIDEA enhances PPAR $\gamma$   
binding to a UCP1  
enhancer element to drive  
UCP1 transcription

Jash et al., iScience 20, 73–89  
October 25, 2019 © 2019 The  
Author(s).  
[https://doi.org/10.1016/  
j.isci.2019.09.011](https://doi.org/10.1016/j.isci.2019.09.011)

## Article

# CIDEA Transcriptionally Regulates UCP1 for Britening and Thermogenesis in Human Fat Cells

Sukanta Jash,<sup>1</sup> Sayani Banerjee,<sup>1</sup> Mi-Jeong Lee,<sup>2</sup> Stephen R. Farmer,<sup>3</sup> and Vishwajeet Puri<sup>1,4,\*</sup>

## SUMMARY

**Our study identifies a transcriptional role of cell death-inducing DNA fragmentation factor-like effector A (CIDEA), a lipid-droplet-associated protein, whereby it regulates human adipocyte britening/beiging with consequences for the regulation of energy expenditure. The comprehensive transcriptome analysis revealed CIDEA's control over thermogenic function in brite/beige human adipocytes. In the absence of CIDEA, achieved by the modified dual-RNA-based CRISPR-Cas9n<sup>D10A</sup> system, adipocytes lost their britening capability, which was recovered upon CIDEA re-expression. Uncoupling protein 1 (UCP1), the most upregulated gene in brite human adipocytes, was suppressed in CIDEA knockout (KO) primary human adipocytes. Mechanistically, during induced britening, CIDEA shuttled from lipid droplets to the nucleus via an unusual nuclear bipartite signal in a concentration-dependent manner. In the nucleus, it specifically inhibited LXR $\alpha$  repression of UCP1 enhancer activity and strengthened PPAR $\gamma$  binding to UCP1 enhancer, hence driving UCP1 transcription. Overall, our study defines the role of CIDEA in increasing thermogenesis in human adipocytes.**

## INTRODUCTION

The identification and characterization of brite/beige (a.k.a. brown-like) adipocytes has drawn considerable attention, as these cells are thought to regulate energy production and may help combat obesity and insulin resistance (Nedergaard and Cannon, 2010; Vernochet et al., 2010). Adult humans possess brown adipocytes that are activated by cold stimuli via the sympathetic nervous system (Nedergaard et al., 2007; Nedergaard and Cannon, 2010, 2013). Progenitors isolated from subcutaneous white fat from children or adults can be induced to acquire a brite phenotype (Ahmadian et al., 2011; Fisher et al., 2012; Ohno et al., 2012), characterized by enhanced oxygen consumption and expression of uncoupling protein 1 (UCP1) and cell-death inducing DNA fragmentation factor-like effector A (CIDEA).

CIDEA downregulates UCP1 activity in brown adipose tissue (Zhou et al., 2003). Originally thought to be a mitochondrial protein, CIDEA was later discovered to be a lipid droplet (LD)-associated protein (Christianson et al., 2010; Puri et al., 2008; Reynolds et al., 2015) not localized to mitochondria in adipocytes. Unlike in mice (Zhou et al., 2003), CIDEA expression in human adipocytes correlates with insulin sensitivity (Puri et al., 2008) and lipid disorders in obese patients (Feldo et al., 2013). Furthermore, a CIDEA polymorphism has been associated with a clinical metabolic phenotype (Dahlman et al., 2005; Nordstrom et al., 2005; Wu et al., 2013; Zhang et al., 2008). CIDEA is endogenously expressed in human but not in rodent white adipocytes. A study by Kulyte et al. provided a strong rationale to our study where they have shown that CIDEA localizes in both the cytoplasm and the nucleus and it binds to liver X receptors (LXR) to regulate their activity in human white adipocytes (Kulyte et al., 2011). Also, CIDEA was found to be expressed at abnormally high levels in white adipose tissue from cachexic patients and CIDEA overexpression *in vitro* inhibited glucose oxidation while stimulating fatty acid oxidation (FAO) (Laurencikiene et al., 2008). Transgenic mice expressing human-CIDEA specifically in adipose tissue show an improved metabolic profile through expansion of adipose tissue (Abreu-Vieira et al., 2015), suggesting that human CIDEA might be functionally different than the mouse CIDEA. Considered a brown adipocyte marker in mice, CIDEA expression increases with britening of mouse white adipocytes (Barneda et al., 2013; Harms and Seale, 2013; Hiraiki et al., 2017; McDonald et al., 2015; Qiang et al., 2012; Seale et al., 2007, 2008; Vernochet et al., 2009; Wang et al., 2016). Beyond its associations with thermoregulation (Barneda et al., 2013; Harms and Seale, 2013; McDonald et al., 2015; Qiang et al., 2012; Seale et al., 2007; Vernochet et al., 2009), lipid droplet dynamics, and lipid metabolism (Barneda et al., 2015; Puri et al., 2008; Wu et al., 2014), little is known about the molecular role of CIDEA in britening and thermogenesis of human adipocytes.

<sup>1</sup>Department of Biomedical Sciences and Diabetes Institute, Heritage College of Osteopathic Medicine, Ohio University, Athens, OH 45701, USA

<sup>2</sup>Icahn School of Medicine, Mount Sinai, New York, NY, USA

<sup>3</sup>Department of Biochemistry, Boston University School of Medicine, Boston, MA 02118, USA

<sup>4</sup>Lead Contact

\*Correspondence: puri@ohio.edu

<https://doi.org/10.1016/j.isci.2019.09.011>



To delineate the association of CIDEA with thermogenesis in humans, we established a positive correlation of CIDEA and UCP1 expression in britened human adipose tissue. We then used human primary white adipose tissue-derived stromal vascular cells (hADSCs) as a model system and developed dual RNA-based CRISPR-Cas9 system to knock out CIDEA in primary human cells. We also developed a modified RNA methodology for dose-dependent expression of CIDEA in human adipocytes. Brite adipocytes exhibited elevated UCP1 expression and increased mitochondrial biogenesis along with brite/beige markers. Our studies reveal that during britening CIDEA expression increases and it translocates to the nucleus via a nuclear bipartite signal. In the nucleus, CIDEA induces a brite phenotype in human adipocytes by transcriptional regulation of UCP1 via directly interacting with Liver X Receptor alpha,  $LXR\alpha$ , and weakening its binding to UCP1 enhancer. Our studies also identified that CIDEA strengthened PPAR $\gamma$  binding to UCP1 enhancer. Overall, our study identifies a molecular mechanism of CIDEA-mediated regulation of britening and maintenance of brite phenotype in primary human adipocytes.

## RESULTS

### CIDEA Expression in Human Brite Adipose Tissue Correlates with UCP1 Expression

Treatment of subcutaneous white adipose tissue explants from five obese human subjects with 1  $\mu$ M rosiglitazone (Rosi) for 7 days induced CIDEA and UCP1 expression reliably (Figure S1A). An average 2.5-fold increase in CIDEA expression correlated with an ~55-fold increase in UCP1 expression, which was negligible without treatment. This britening process was independent of demographics and body mass index. These preliminary studies complimented the role of CIDEA in healthy metabolic phenotype in humans (Dahlman et al., 2005; Feldo et al., 2013; Gummesson et al., 2007; Nordstrom et al., 2005; Puri et al., 2008; Wu et al., 2013; Zhang et al., 2008).

### Modified CRISPR-Cas9nD10A Methodology to Knock Out CIDEA in Cultured Human Primary Adipocytes

To study the loss of function of CIDEA in human primary cells, we established a modified efficient genome engineering method for genetic manipulation in adipocytes differentiated from hADSC. We modified the existing CRISPR/Cas9 system to knock out CIDEA in multipotent human adipose-derived stromal progenitor cells (hADSCs) from freshly isolated human subcutaneous adipose tissue. To achieve an efficient CIDEA knockout (KO), we designed multiple single guide RNA (sgRNA) in combination of Cas9 or its mutated form to target the CIDEA gene loci (Figure 1A; also see Figures S1, S2, and S3A–S3C and Supplemental Information). With our modified CRISPR-Cas9nD10A nickase methodology, we were able to knock out CIDEA in human adipocytes (Figure 1B).

We next developed a modified-mRNA methodology to perform gain-of-function studies (Figure S3D). Modified codon-optimized CIDEA mRNA (mcom CIDEA-mRNA; also called CIDEA mod mRNA) produced eloquent dose- and time-dependent control of CIDEA expression within physiological limits (Figures 1C and 1D; also see Methods and Figures S3E–S3G). In all our further studies, 1–2  $\mu$ g mcom CIDEA-mRNA was used.

### Thiazolidinedione-Induced Human Adipocyte Britening

Human brite adipocytes, termed T-brites, were obtained by treating mature white adipocytes, that had been differentiated from hADSCs (Lee et al., 2012, 2013), with 1  $\mu$ g/mL Rosi for 7 days. Relative to untreated control cells, T-brites had increased mRNA expression of PPAR $\gamma$  target genes (*ADIPOQ*, *FABP3*, *FABP4*, and *RXRA*) and brite/beige marker genes (*PGC1 $\alpha$ / $\beta$* , *PRDM16*, *CEBP $\beta$* , *CIDEA*, and *ELOVL3*), without expression changes in lipogenic genes (*FASN* and *SCD1*) (Figures S4A and S4B). Notably, T-brites exhibited an 85-fold increase in *UCP1* mRNA expression (Figure S4C) together with increased mRNA expression of other brite marker genes (*CITED*, *TBX1*, *MTUS1*, and *KCNK3*) (Figure S4D). We did not detect changes in the transcription of brown or white marker genes (Figures S4E and S4F, respectively). Induction of *PGC1 $\alpha$*  and *PGC1 $\beta$*  transcription in T-brites was accompanied by increased transcription of mitochondrial complex I–V components (Figure S4G).

T-brites showed upregulated *PLIN1* and *ATGL* transcription but downregulated transcription of *ATGL*'s inhibitor *G0S2* (Figure S4H). Meanwhile, mRNA levels of *FSP27*, which negatively regulates lipolysis (Grahm et al., 2014; Singh et al., 2014), were unchanged in T-brites, perhaps due to positive regulation by Rosi (Puri et al., 2007, 2008). T-brites exhibited upregulated mRNA expression of acyl coenzyme A

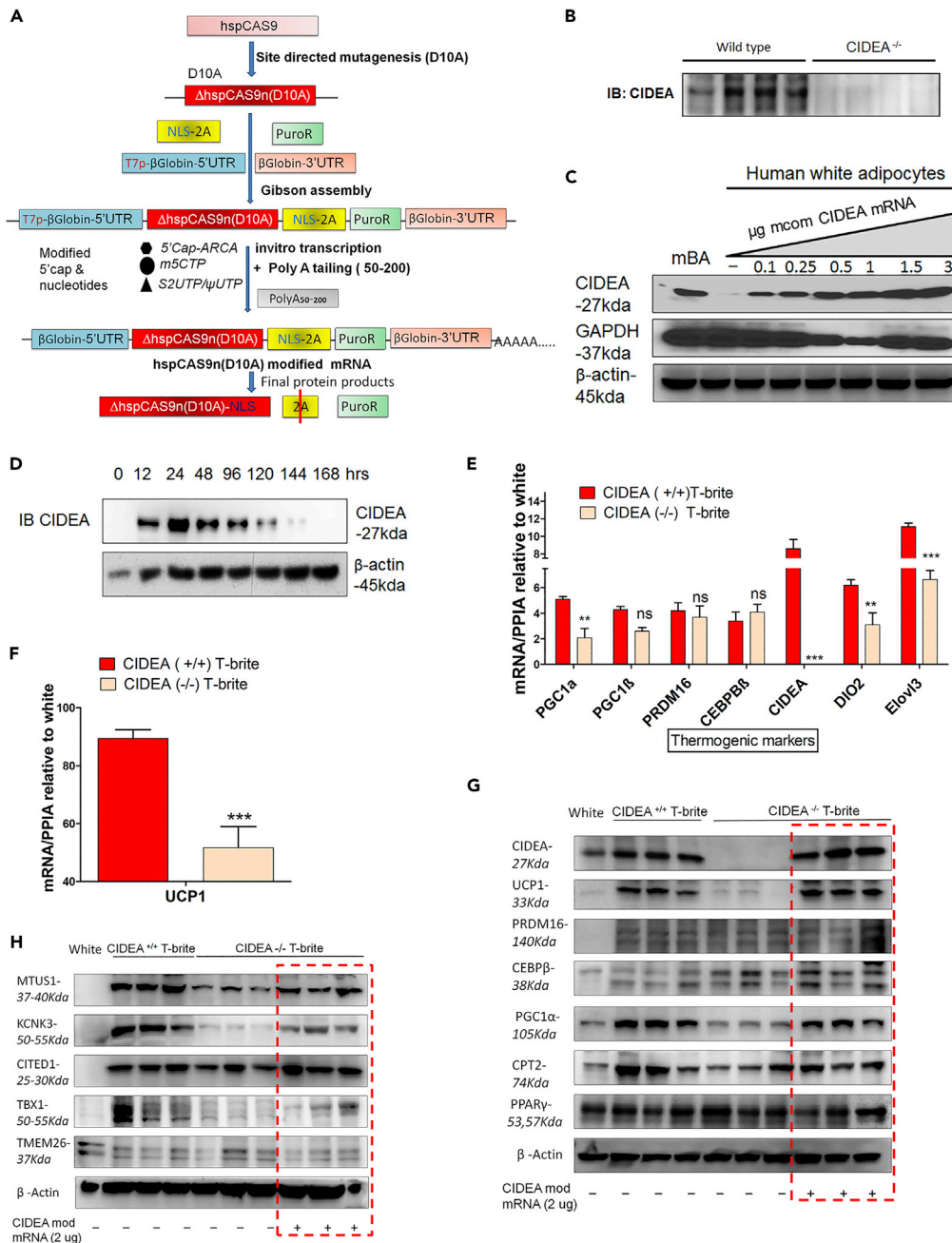


**Figure 1. CIDEA KO Inhibits Britening of Human White Adipocytes**

(A) CRISPR-Cas9 construction. Hybrid Cas9 construct (Cas9<sup>D10A</sup>-2A-P) and modified human Cas9 mRNA synthesis workflow.

(B) Western blot showing CRISPR-Cas9D10A nickase-mediated abolishment of CIDEA in four biallelic clones of mature adipocytes.

(C) CIDEA protein expression profile after dose-dependent mcom CIDEA mRNA single transfection (24 h) into human white adipocytes. Mouse brown adipocyte (mBA) lysate was blotted as a positive control.

(D) Time course expression profile of mcom CIDEA mRNA after single transfection into Hek293T cells. Modified codon-optimized CIDEA mRNA (mcom CIDEA-mRNA; also called CIDEA mod mRNA) produced eloquent dose- and time-dependent control of CIDEA expression (C and D).

(E and F) Expression of thermogenic genes (E) and UCP1 (F) in Rosi-treated WT (CIDEA<sup>+/+</sup>) and KO (CIDEA<sup>-/-</sup>) T-brites derived from hADSCs. CIDEA<sup>-/-</sup> cells were derived from WT hADSCs by CRISPR-CAS9-mediated KO. Data are expressed as fold changes over dimethyl sulfoxide (DMSO; vehicle)-treated adipocytes, and each data point represents pooled cell

**Figure 1. Continued**

fractions from three individual donors. Data are mean  $\pm$  SEM (n = 3). \*\*\*p < 0.001, and \*\*p < .01, two-way ANOVA followed by Bonferroni post tests.

(G and H) Protein expression of thermogenic (G) and brite genes (H) in CIDEA<sup>+/+</sup> and CIDEA<sup>-/-</sup> T-brites treated with Rosi. After 7 days of Rosi, CIDEA<sup>-/-</sup> adipocytes were transfected with GFP control mRNA or mcom-CIDEA mRNA (red box) to re-express CIDEA for 3 days. Each lane in the red box represents an individual CIDEA<sup>-/-</sup> clone.

dehydrogenase genes (VLCAD, LCAD, MCAD) and other FAO-associated genes (PPAR $\alpha$ , CPT1, CPT2) (Figure S4I). The mRNA abundances of TCA cycle enzyme genes (MDH2 and IDH3a) were also increased in T-brites (Figure S4J). T-brites were found to have elevated mitochondrial DNA contents (data not shown), consistent with increased mitochondrial biogenesis and activity, accompanied by increased FAO and TCA cycle entry characteristic of uncoupling events leading to thermogenesis.

**Absence of CIDEA Inhibits Britening and Uncoupling in Human Adipocytes**

As predicted, CIDEA expression was plentiful in CIDEA<sup>+/+</sup> T-brites produced by Rosi induction (Figure 1E). By comparison, CIDEA<sup>-/-</sup> T-brites produced by CRISPR-Cas9 KO in hADSCs had reduced PGC1 $\alpha$ , DIO2, Elov13, and UCP1 mRNA expression (Figures 1E and 1F), with no significant changes in PGC1 $\beta$ , PRDM16, and CEBP $\beta$  mRNA expression (Figure 1E). Other brite genes were reduced in CIDEA<sup>-/-</sup> T-brites (Figure S5A). BAT markers (Figure S5B) and lipogenic genes (FASN and SCD1; data not shown) were unaffected by CIDEA KO. Expression of the FAO regulatory genes CPT1 and CPT2 was decreased, whereas PPAR $\alpha$ , VLCAD, LCAD, and MCAD mRNA levels were unaltered (Figure S5C). Britening-induced increases in mitochondrial DNA copy number were unaffected by CIDEA KO (Figure S5D). Select electron transport chain genes were downregulated in CIDEA<sup>-/-</sup> T-brites (Figure S5E), whereas adipogenic gene expression did not differ between CIDEA<sup>+/+</sup> and CIDEA<sup>-/-</sup> T-brites (data not shown). CIDEA KO reduced protein expression of PGC1 $\alpha$  (PPAR $\gamma$  coactivator 1 alpha), UCP1, CPT (carnitine palmitoyltransferase) 2, CITED (Cbp/P300 interacting transactivator with Glu/Asp-rich carboxy-terminal domain), MTUS (microtubule-associated scaffold protein)1, TBX1 (T-box 1), and KCNK3 (potassium two-pore domain channel subfamily K member 3) but not PPAR $\gamma$ , PRDM16 (PR domain containing 16), CEBP $\beta$  (CCAAT/enhancer-binding protein beta), and TMEM (TransMEMbrane protein); these reductions were reversed by CIDEA re-expression (Figures 1G and 1H, red box). These results suggest that CIDEA plays an important role in adipocyte britening via regulation of thermogenic genes.

**CIDEA KO Diminishes Increased OCR in T-Brites**

The basal oxygen consumption rate (OCR) was higher in T-brites than in white adipocytes (Figure 2A). Relative to non-KO controls, CIDEA<sup>-/-</sup> T-brites had reduced mitochondrial respiration, proton leakage, and maximal respiratory capacity (Figure 2B) but unchanged coupling efficiency and thus unchanged mitochondrial energy production (Figure S6A). These data revealed that irrespective of britening or CIDEA's absence, the efficiency of mitochondrial energy production, above the oligomycin-mediated ATP-block, was same under basal conditions. The cell respiratory ratio (cRCR), a respiratory capacity index, was higher in T-brites than in white adipocytes (Figure S6B). CIDEA KO did not change cRCR, arguably owing to reduced substrate oxidation and proton leakage because cRCR is sensitive to these factors but insensitive to ATP turnover.

**CIDEA-Mediated Increase in OCR Is UCP1 Dependent**

CIDEA inhibition has been shown to increase stimulated lipolysis, thus increasing free fatty acids (FFAs) (Puri et al., 2008). We found that basal lipolysis was increased in CIDEA<sup>-/-</sup> adipocytes (Figure S2E). Excessive production of intracellular FFAs during lipolysis can mask UCP1-mediated leak respiration through non-specific protonophoric FFA actions and mitochondrial permeability transition pore (PTP) opening (Li et al., 2014). Therefore, we compared T-brite OCRs in wild-type (WT) CIDEA<sup>+/+</sup> versus KO CIDEA<sup>-/-</sup> T-brites stimulated with isoproterenol (ISO), to differentiate CIDEA's involvement in UCP1 activity versus PTP-mediated leak respiration. Injection of T-brites at 30 min time point with the  $\beta$ -adrenoreceptor agonist ISO (to increase endogenous FFAs) increased OCR, with or without CIDEA (Figures 2C and 2D). Maximization of oxidative capacity with the protonophore FCCP [carbonyl cyanide-4-(trifluoromethoxy)phenylhydrazone] during ISO-induced OCR was lower in CIDEA<sup>-/-</sup> than in CIDEA<sup>+/+</sup> T-brites, evidencing a contribution of CIDEA to mitochondrial reserve capacity and uncoupling (Figure 2C). ISO-induced ATP-linked respiration showed no significant difference in CIDEA<sup>-/-</sup> and CIDEA<sup>+/+</sup> T-brites (Figures 2C and 2D), indicating that proton leak was masked in CIDEA<sup>-/-</sup> cells. Therefore, to assess UCP1's contribution to uncoupled

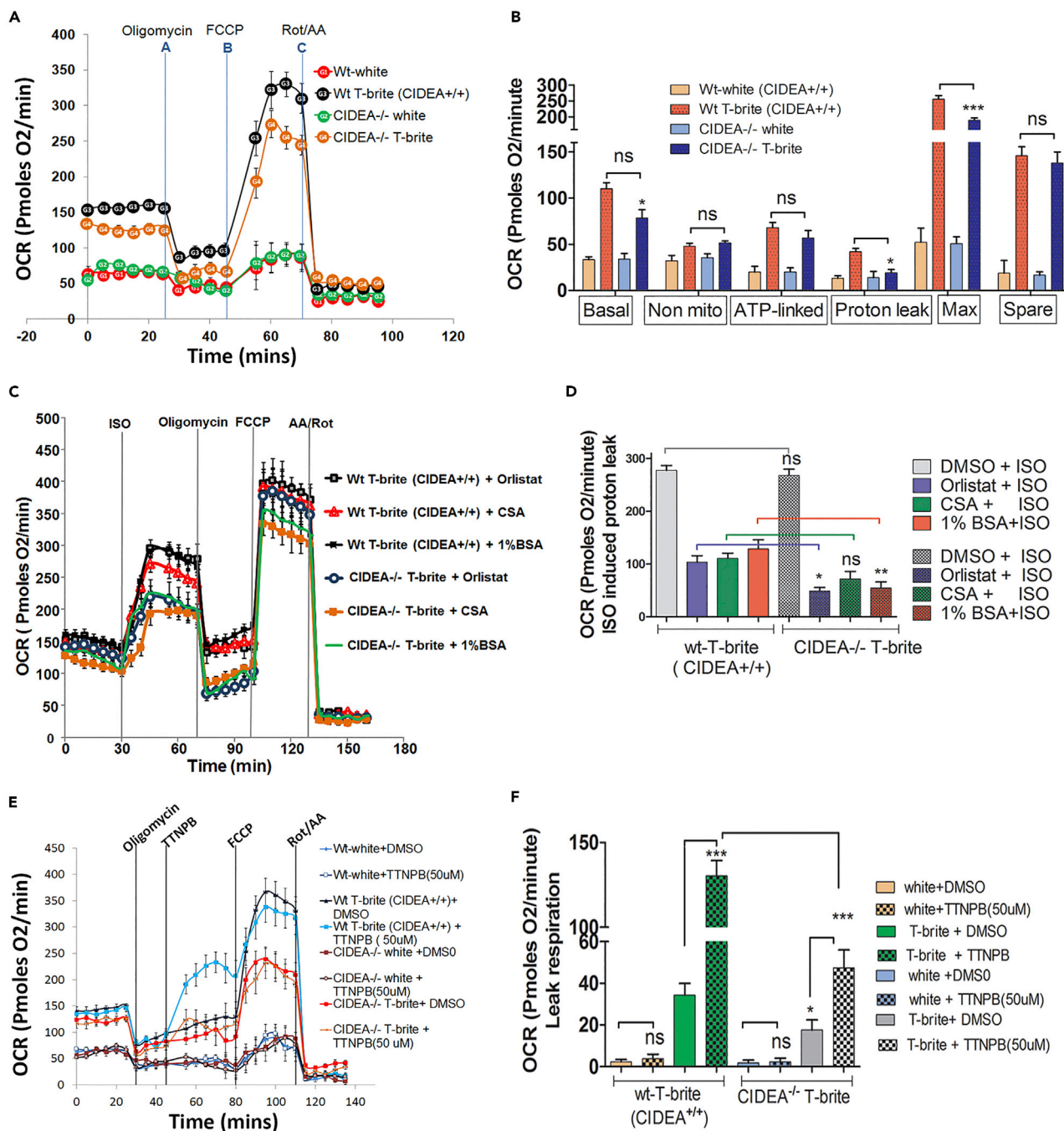


**Figure 2. CIDEA KO Inhibits UCP1-dependent OCR in Human Adipocytes Induced for Britening**

(A) Seahorse bioanalyzer respirometry of differentiated WT and CIDEA<sup>-/-</sup> white adipocyte and T-brites show basal respiration, proton leak respiration (after 2 μm oligomycin treatment), maximal substrate oxidation (12 μm FCCP), and non-mitochondrial respiration (5 μm/5 μm antimycin A/rotenone). All data points are an average of 8–10 wells.

(B) Quantification of basal respiration, ATP turnover, proton leak, and maximum respiratory capacity of the samples in panel (A).

(C) Bioenergetics of ISO-induced OCR of WT and CIDEA<sup>-/-</sup> T-brites pretreated with vehicle (DMSO) or FFA-induced leak respiration blocker (2 h, 20 μm orlistat; 12 h, 6 μg/mL CSA; 1% BSA).

(D) Lipolysis suppression, PTP blockade, or FFA scavenging inhibited ISO-induced leak respiration in CIDEA<sup>-/-</sup> T-brites.

(E) Time course OCR of WT and CIDEA<sup>-/-</sup> white and brite/beige adipocytes treated with 50 μM arotinoid acid (TTNPB) or DMSO or after basal and oligomycin-dependent respiration. FCCP and antimycin A/rotenone were added subsequently.

(F) TTNPB increased uncoupled/leak respiration in brite/beige cells in UCP1-dependent manner.

Data in (B), (D), and (F) are mean ± SEM (n = 3). \*\*\*p < 0.001 and \*\*p < .01, two-way ANOVA followed by Bonferroni post tests.

T-brite respiration, we suppressed excess FFA-mediated proton leakage via PTPs with a pretreatment with the lipase inhibitor orlistat, the PTP blocker cyclosporin A (CSA) or the FFA sink BSA (BSA, 1%). The reducing effects of orlistat and 1% BSA on PTP-dependent (UCP1-independent) proton-leak respiration were more pronounced in CIDEA<sup>-/-</sup> than in CIDEA<sup>+/+</sup> T-brites, implicating UCP1 dependence in CIDEA-mediated increases in OCR; the CSA effect did not differ significantly between WT and KO cells (Figures 2C and 2D). Taken together, these results showed that CIDEA KO reduced UCP1-dependent uncoupled respiration.

To further assess the direct contribution of UCP1 to OCR, we administered UCP1 activator, TTNPB (the retinoid analog), after inhibiting coupled oxygen consumption with oligomycin. Because TTNPB increases proton conductance through the inner mitochondrial membrane, we hypothesized that the number of UCP1 molecules present in the inner mitochondrial membrane might correlate with TTNPB-mediated increased respiration. After dose optimization for OCR augmentation without cytotoxicity (data not shown), 50  $\mu$ M TTNPB was found to have a more robust OCR augmentation effect on oligomycin-inhibited CIDEA<sup>+/+</sup> T-brites than on CIDEA<sup>-/-</sup> T-brites (Figures 2E and 2F); white adipocytes did not respond to TTNPB. CIDEA's role in UCP1-mediated OCR was further confirmed when CIDEA re-expression in CIDEA<sup>-/-</sup> cells, using CIDEA mcomRNA, restored the TTNPB-induced increase in respiration to nearly the level of control T-brites (Figures S6C and S6D). TTNPB did not alter FCCP efficacy, suggesting different modes of action for the two agents (Figure 6C). Finally, elevated oxidative phosphorylation subunit levels in T-brites, compared with white adipocytes, were decreased by CIDEA KO and recovered with CIDEA re-expression (Figure S6E).

### CIDEA Is Critical for Adipocyte Britening by Various Inducers

To confirm that the role of CIDEA in britening was not specific to Rosi, britening of mature human white adipocytes was induced with a 7-day exposure to 1 nM CL316,243 (a  $\beta$ 3 agonist), 100 nM fibroblast growth factor 21 (FGF21), or 100 nM atrial natriuretic peptide (ANP; dosage optimization data not shown) in the presence or absence of CIDEA and confirmed by the characteristics of high mitochondrial content, UCP1 expression, and thermogenic capacity (Bordicchia et al., 2012; Ghorbani and Himms-Hagen, 1997; Granneman et al., 2005). In all cases, levels of transcripts encoding UCP1, PGC1 $\alpha$ , CIDEA, PRDM16, and CPT2 transcript levels were robustly increased relative to levels in white adipocytes (Figure S7A). In addition to reducing UCP1 transcription in response to these inducers, KO of CIDEA was associated with lesser induction of several thermogenic and brite marker mRNAs (precise effects varied among inducers, see Figure S7A). Consistent with these mRNA expression data, CIDEA<sup>-/-</sup> T-brites had lower UCP1, PGC1 $\alpha$ , MTUS1, and CITED1 protein expression than CIDEA<sup>+/+</sup> T-brites (Figure S7B). In consonance with our previous finding of CIDEA's role in LD morphology (Christianson et al., 2010; Puri et al., 2008), relative to CIDEA<sup>+/+</sup> T-brites, CIDEA<sup>-/-</sup> T-brites had reduced LD sizes after being treated with britening inducers (Figure S8A).

CIDEA KO rendered britening activators less effective at raising UCP1-dependent OCR (in the presence of a PTP inhibitor) (Figure S8B). ISO-induced proton leakage (respiratory uncoupling) was also reduced in CIDEA<sup>-/-</sup> T-brites in the presence of the PTP inhibitor (Figure S8C). Similar results were obtained in the presence of 1% BSA, which was used to mask non-specific FFA effects (Figures S8D and S8E). These results suggested that CIDEA acts as a regulator of human adipocyte britening, independent of the induction pathway triggered.

### Transcriptome Analysis in Britened Human White Adipocytes in the Presence and Absence of CIDEA

To perform transcriptome analysis, we transdifferentiated white adipocytes into brite adipocytes with a cocktail containing Rosi, FGF21, ANP, and  $\beta$ 3 agonist. The idea was to examine the global effect of britening and thermogenic response in CIDEA<sup>-/-</sup> and CIDEA<sup>+/+</sup> T-brites. We identified unique gene signature of brite or thermogenic genes affected by the complete absence of CIDEA (Figure 3A). Differential gene expression analysis with applied filters (ANOVA  $p < 0.05$  and linear fold change  $< -2$  or  $.2$ ) revealed upregulation of 1,757 genes and downregulation of 1,982 genes in the CIDEA<sup>-/-</sup> T-brite adipocytes. Furthermore, expression clustering of selected highly downregulated (Figure 3B) and highly upregulated (Figure 3C) genes in the CIDEA<sup>-/-</sup> T-brites indicate CIDEA's control over thermogenic and metabolic functions. The differentially expressed genes were categorized by gene ontology analysis (GO) followed by DAVID analysis (Figure 3D). The GO analysis revealed that genes involved in overall thermogenic functions including adaptive thermogenesis (GO:1990845), fatty acid oxidation (GO:0019395), mitochondrial

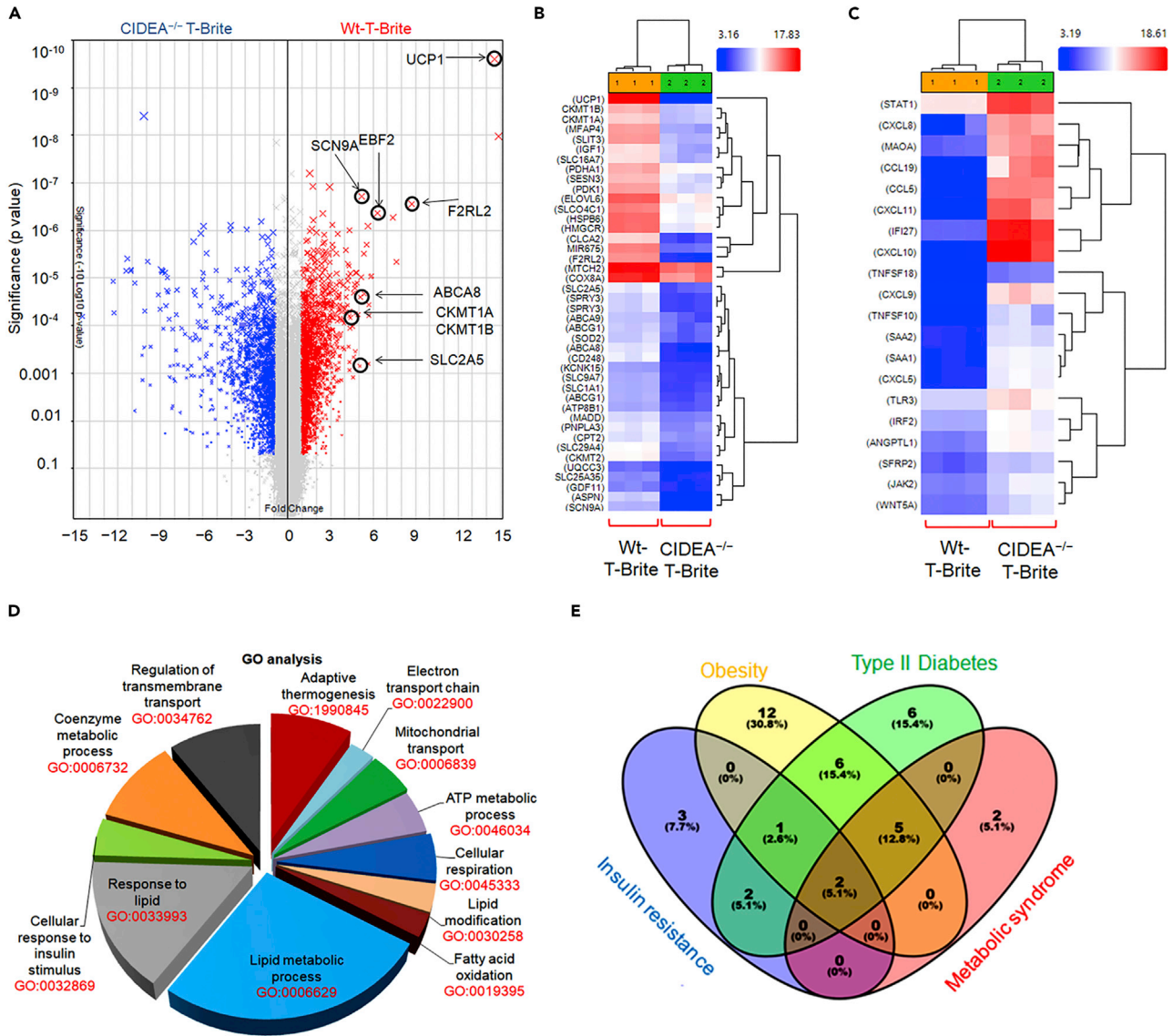


**Figure 3. A Whole-Genome Transcriptome Microarray Analysis of T-brite Adipocytes ± CIDEA**

(A) Volcano plot from hierarchical clustering of differentially expressed genes in T-brite human adipocytes ± CIDEA (n = 3 in each group). Plot demonstrates a decrease in defined thermogenic (UCP1, EBF2, CKMT1A, CKMT1B) and transmembrane markers in T-brite adipocytes in the absence of CIDEA. UCP1 was most upregulated upon browning of human white adipocytes in the presence of CIDEA.

(B) Heatmap of select highly downregulated genes in T-brite adipocytes in the absence of CIDEA (Fold enrichment ≥ 3.8, p < 0.05).

(C) Heatmap of select highly upregulated genes in T-brite adipocytes in the absence of CIDEA (Fold enrichment ≥ 4.5, p < 0.05).

(D) Pathway analysis of differentially regulated genes. Analysis of select GO terms enriched in the differentially regulated genes, downregulated in CIDEA-KO T-brites compared with the wild-type T-brites, with fold changes ≥ 3.85 (p < 0.05). The number on each pie slice indicates the number of genes in the respective GO terms.

(E) Venn Diagram analysis of individual GAD disease gene sets (colored circles) from the corresponding downregulated (Fold enrichment ≥ 3.8, p < 0.05) genes in CIDEA-KO T-brites.

All Venn Diagrams were produced with Venny <http://bioinfogp.cnb.csic.es/tools/venny/index.html>. The numbers on the Venn diagram indicate the number of genes shared or unshared between the indicated disease.

transport (GO:0006839), electron transport chain (GO:0022900), cellular respiration (GO:0045333), ATP metabolic process (GO:0046034), coenzyme metabolism (GO:0006732), response to lipid (GO:0033993), and response to insulin stimulation (GO:0032869) were also downregulated in the CIDEA<sup>-/-</sup> T-brite group. In addition to the downregulation of well-established gene network related to thermogenic function, CIDEA<sup>-/-</sup> T-brites showed suppression of Creatine kinase (CKMT1) expression. Recently, CkMT1-driven

creatine cycle has been shown to be involved in UCP1-independent brite adipocyte thermogenic program (Kazak et al., 2015). This analysis indicated a possible role of CIDEA in thermogenesis in the brite adipocytes.

Next, we categorized the highly downregulated gene sets in CIDEA<sup>-/-</sup> T-brite adipocytes to the human genetic association database (GAD) to identify the significance of CIDEA in beige adipocyte function with the related metabolic disease. GAD primarily links common complex human disease rather than rare Mendelian inheritance in man (OMIM). GAD analysis indicated common metabolic disease linked to highly downregulated genes in CIDEA<sup>-/-</sup> T-brite adipocytes. Venn diagram comparison among related GAD disease showed modest gene sharing as shown in Figure 3E. This disease-related sharing at the gene level suggests a common regulatory mechanism governing browning/thermogenesis, obesity, insulin resistance, type II diabetes, and metabolic syndrome. Interestingly, CIDEA polymorphism is well connected with metabolic syndrome in humans (Dahlman et al., 2005; Nordstrom et al., 2005; Wu et al., 2013; Zhang et al., 2008). Indeed, a recent study showed that human-CIDEA specifically expressed in mouse adipose tissue improves whole-body metabolic phenotype (Abreu-Vieira et al., 2015).

### CIDEA Nuclear Localization Depends on a Bipartite Nuclear Localization Signal

CIDEA expression started increasing after 12 h upon browning induction and plateaued at 144 h (Figure S9A). Subcellular fractionation revealed nuclear localization of CIDEA beginning 24 h and peaking 48 h after browning induction (Figure 4A). Perilipin (PLIN1; negative control) remained in the lipid fraction throughout the process. Interestingly, CIDEA enrichment in the nucleus increased 5 h after ISO treatment (Figure 4B). This localization was blunted by a simultaneous cycloheximide treatment (Figure S9B). During ISO treatment, FFA/BSA blocked nuclear enrichment but enhanced CIDEA concentrations in the lipid fraction (Figure 4C). These results suggest that shuttling of CIDEA from LDs to the nucleus depends on its concentration and lipid availability. A competitive assay in which LD-associated CIDEA was saturated with 3×HA-CIDEA-mcomRNA before adding 6×His-CIDEA mcomRNA showed that, at a fixed saturable concentration of 3×HA-CIDEA, 6×His-CIDEA was enriched dose dependently in CIDEA<sup>-/-</sup> T-brite nuclei (Figure 4D). In fact, the localization of 6×His-CIDEA suggested retrograde nucleus-to-LD shuttling of CIDEA. Bipartite nuclear localization signal (NLS) mapping demonstrated that the 21–49 amino acid (aa) region of human CIDEA, which contains two basic aa clusters separated by a 21-aa spacer, has a high nuclear score of 4.0 (Figure 4E). Similar sequence in mouse and rat showed lower nuclear score. This indicates a high probability of nuclear localization of human CIDEA. Deletion of the NLS (1–219ΔNLS) or substitution of a key lysine (K23A) or arginine (R44A) disrupted CIDEA nuclear localization (Figure 4F), whereas mutation of unrelated arginines (R13A, R127A) did not (data not shown), demonstrating NLS specificity for nuclear localization. These results confirm the importance of bipartite NLS for nuclear entry of human CIDEA.

We tested whether CIDEA translocation to the nucleus depends on passive diffusion through nuclear pore complexes or  $\alpha/\beta$  importin-Ran-GTPase-mediated active transport. The  $\alpha/\beta$  importin inhibitor ivermectin did not affect CIDEA nuclear import, indicating that it does not require active transport via  $\alpha/\beta$  importin-Ran-GTPase, but blocked the import of HA-t-Ag containing a monopartite NLS recognized by  $\alpha/\beta$  importin (Figure S9C). Apyrase, a nucleotide hydrolase, reduced nuclear import of CIDEA (Figure S9C). These data suggest that CIDEA nuclear entry is at least partially ATP dependent, perhaps facilitated by NLS-binding carrier molecules or may be via protein piggybacking.

### CIDEA Is a Transcriptional Activator of UCP1 during Browning

We next identified the region of UCP1 promoter/enhancer associated with CIDEA-mediated regulation of UCP1 transcription. Experiments with various luciferase-UCP1 constructs (Figure 5A) showed that the 150-bp proximal minimal region of the UCP1 distal enhancer was crucial for CIDEA-mediated upregulation of UCP1 distal enhancer activity (Figure 5B). Interestingly, this region contains previously characterized DR4 and DR1 sequences; LXR binds DR4 to downregulate UCP1 expression, whereas PPAR $\gamma$  binds DR1 to upregulate UCP1 expression (Juge-Aubry et al., 1997; Wang et al., 2008). Therefore, to examine whether CIDEA-mediated UCP1 regulation depends on the DR1 or DR4 sequences, we generated DR1 and DR4 loss of function mutation on 150 bp proximal enhancer sequence (Figure 5C; top three rows). Addition of CIDEA mcomRNA activated the intact minimal distal enhancer (Figure 5D, DR4-DR1). Deletion of DR1 abrogated enhancer activity completely, whereas deletion of DR4 increased enhancer activity, independent of exogenous CIDEA (Figure 5D), suggesting that DR4-LXR binding might mediate CIDEA upregulation of UCP1. To further delineate the association of CIDEA with the DR4 element, we generated

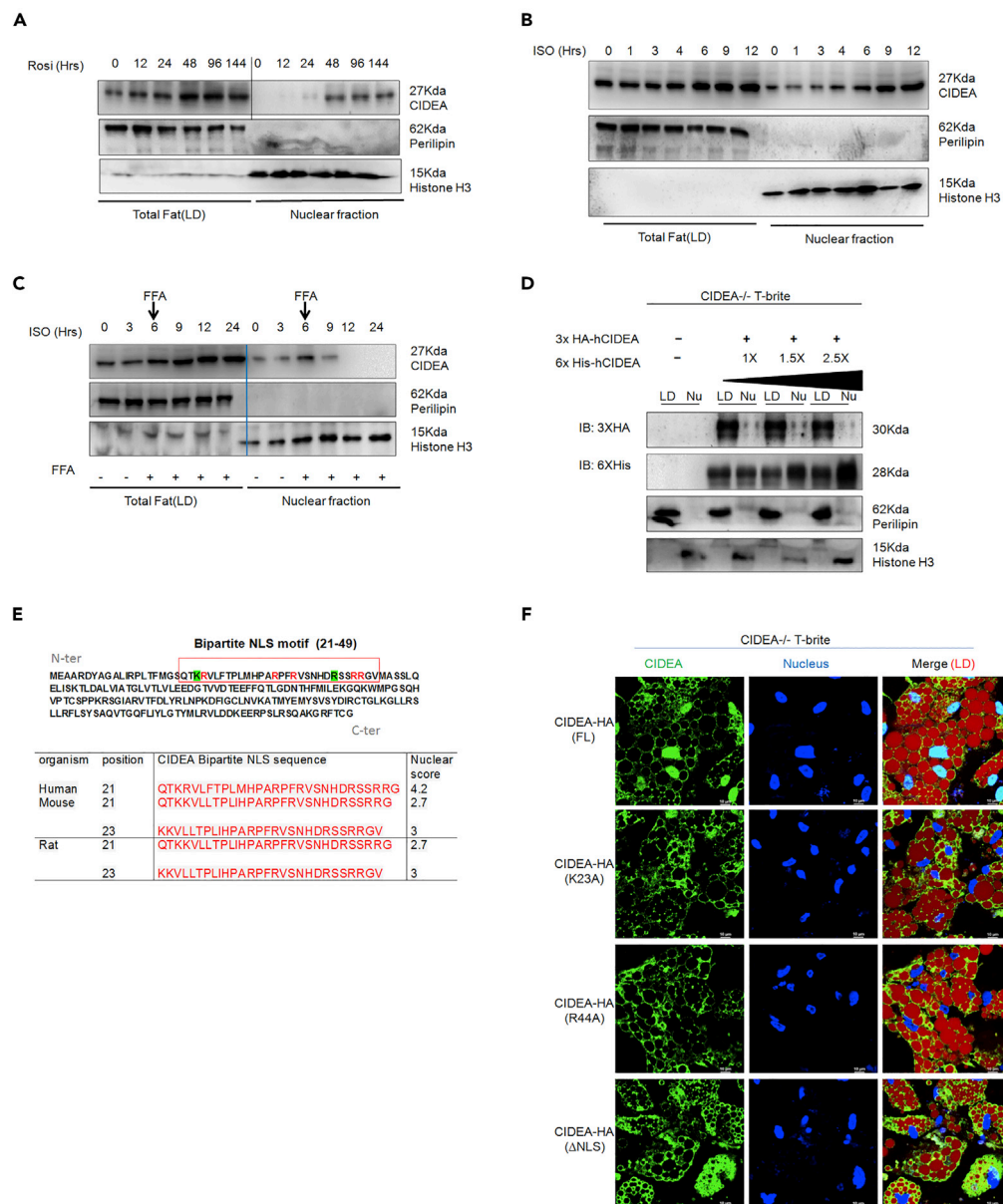


**Figure 4. Nuclear Shuttling of CIDEA**

(A) Time courses of CIDEA protein expression in human white adipocytes after addition of 1  $\mu$ m Rosi.  
 (B) Time-dependent LD versus nuclear enrichment of CIDEA after ISO-induction of T-brites.  
 (C) Compartmentalization of CIDEA in LDs and nuclei after albumin-bound FFA-mix challenge 6 h after ISO induction. FFA-mix (FFA/BSA) challenge inhibited CIDEA nuclear accumulation with concomitant LD enrichment.  
 (D) Competitive import assay showing dose-dependent nuclear enrichment of 6 $\times$ His-CIDEA at fixed saturable concentration of 3 $\times$ HA-CIDEA. The CIDEA<sup>-/-</sup> T-brites were transfected initially with 3 $\times$ HA-CIDEA (4  $\mu$ g in each of 6 wells) and then 6 h later with 6 $\times$ His-CIDEA. The cells were harvested 12 h after the last transfection.  
 (E) Top: hCIDEA protein sequence with putative NLS at aa 21–49 (red box). Critical lysine (K23) and arginine (R44) residues are marked green; irrelevant arginines are marked red. Bottom: alignment and comparison of human bipartite NLS with mammalian analogs. Localization prediction scores were obtained from cNLS Mapper.  
 (F) Confocal images showing nuclear and LD localization of HA-tagged FL CIDEA and mutant CIDEA (K23A/R44A substitution or NLS deletion [ $\Delta$ NLS]) in T-brites. Cells were labeled with anti-HA primary antibody followed by AF-488 secondary antibody.

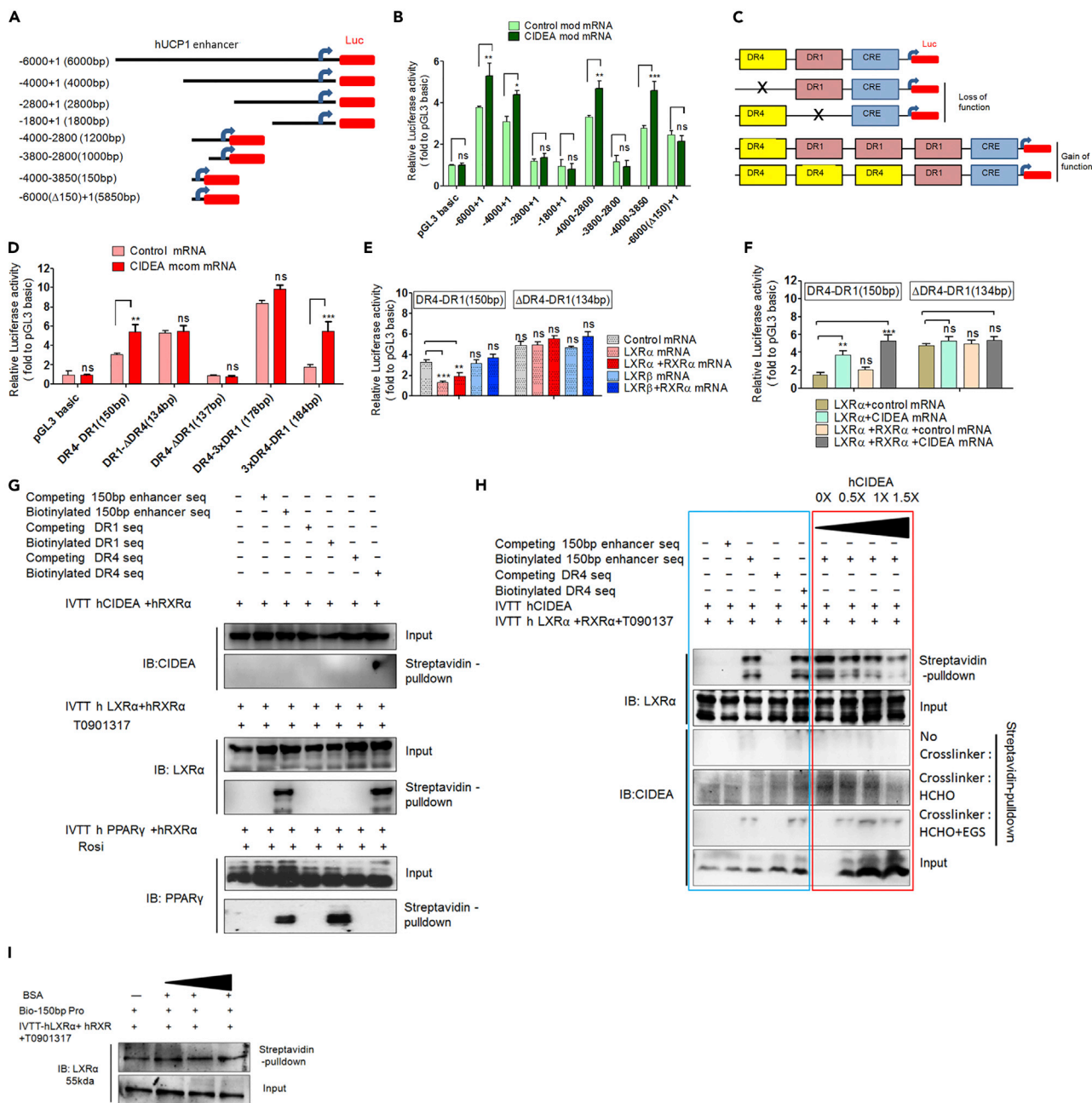


**Figure 5. CIDEA Regulates UCP1 Transcription during Human Adipocyte Britening**

(A) hUCP1-Luc-pGL-3 constructs, including WT (−6,000 to +1) and seven deletion mutant constructs.

(B) Relative luciferase (rLUC) activity of each construct in response to exogenous CIDEA (12 h after transfection of mcom-CIDEA). Constructs were transfected into T-brites 24 h before transfection of mcom-CIDEA (0.750 pg/cell) or control (glyceraldehyde 3-phosphate dehydrogenase [GAPDH]; 0.750 pg/cell) mRNA.

(C) Synthetic dUER<sub>150bp</sub> constructs containing DR1 (PPARγ-binding site) or DR4 (LXR-binding site) were cloned into a pGL-3 LUC vector for functional analysis.

(D) CIDEA (0.750 pg/cell) induction of the UCP1 promoter (150-bp WT, DR1–DR4); the ΔDR1 and ΔDR4 mutations disrupted CIDEA induction in opposite manner.

(E) Exogenous LXRα or LXRα+RXRα mRNA but not LXRβ or LXRβ+RXRα mRNA (all mRNAs: 0.750 pg/cell) suppressed expression of synthetic dUER<sub>150bp</sub> luciferase construct containing WT DR4 (DR4-DR1); this suppression was abolished with mutant DR4 (ΔDR4-DR1).

(F) Effect of exogenous mcom-CIDEA mRNA on rLUC of dUER<sub>150bp</sub> construct. T-brites were transfected with WT or mutant DR4 luciferase constructs 24 h before transfection with CIDEA mRNA (0.750 pg/cell).

**Figure 5. Continued**

(G) *In vitro* biotin-streptavidin DNA pull-down assay for protein-DNA interaction strength assessment of *in vitro* translated human recombinant (r)CIDEA, rLXR $\alpha$ , and rPPAR $\gamma$  to dUER<sub>150bp</sub> or a DR1 or DR4 oligonucleotide. LXR $\alpha$  and PPAR $\gamma$  heterodimeric partner RXR $\alpha$  and their respective ligands were added to facilitate DNA binding. Unlike rLXR and rPPAR, no rCIDEA was pulled down with an equivalent amount of biotinylated DNA as detected by western blotting. (H) Protein-DNA binding analysis of rCIDEA with dUER<sub>150bp</sub> and DR4 in the presence of rLXR $\alpha$  and RXR $\alpha$  (blue box). Interaction strength of rLXR $\alpha$  with dUER<sub>150bp</sub> was reduced with increasing rCIDEA concentration (red box). No CIDEA was recovered by streptavidin pull down followed by western blotting in the absence of a cross-linker. HCHO + EGS cross-linking, but not HCHO-only cross-linking, pulled down CIDEA, revealing a distant CIDEA-LXR $\alpha$  interaction. (I) Progressive addition of BSA (negative control) did not affect LXR $\alpha$ -DR4 interaction. In (B), (D), (E), and (F), data are mean rLUC (relative to pGL-3 basic vector)  $\pm$  SEM (n = 3). \*\*\*p < 0.001, \*\*p < .01, and \*p < .05; two-way ANOVA followed by Bonferroni post tests.

gain-of-function mutants of DR1 and DR4 elements. We speculated that increased number of DR1 or DR4 would enhance the binding of LXR $\alpha$  and PPAR $\gamma$ , respectively. Therefore, we generated two separate 150-bp LUC constructs, one containing three DR4 (3xDR4) with one DR1 element (1xDR1) and other containing three DR1 (3xDR1) with one DR4 element (Figure 5C; bottom two rows). Transfection of 3xDR1:1xDR4 construct resulted in a profound increase in enhancer activity independent of CIDEA, whereas 3xDR4:1xDR1 had no effect on basal enhancer activity, but it robustly responded to exogenous CIDEA (Figure 5D). These results suggest that CIDEA-mediated UCP1 upregulation occurs via DR4, a sequence known to bind LXR to negatively regulate UCP1 expression (Wang et al., 2008).

We next measured UCP1 enhancer activity in the presence of LXR $\alpha$  or LXR $\beta$  alone or with their obligatory heterodimeric partner RXR $\alpha$ . Exogenous LXR $\alpha$ , but not LXR $\beta$ , suppressed UCP1 enhancer activity, consistent with a previous study demonstrating similar selectivity in mice (Wang et al., 2008), and this effect was absent with the deleted-DR4 construct (Figure 5E). Importantly, CIDEA along with LXR $\alpha$  alone or with its obligatory heterodimeric partner RXR $\alpha$  countered this LXR $\alpha$ -mediated suppression of UCP1 enhancer activity (Figure 5F). LXR $\alpha$  agonism with T0901317 reduced UCP1 mRNA expression in CIDEA<sup>-/-</sup> T-brites with or without ISO but only with ISO in CIDEA<sup>+/+</sup> T brites (Figure S10A). Similar results were obtained with GW3965, another LXR agonist (data not shown). We attempted to study the effect of CIDEA by knocking out LXR $\alpha$  by CRISPR, but the LXR $\alpha$  knockout cells did not grow well, showing that LXR $\alpha$  might also have a role in cellular growth and/or development. Therefore, we used small interfering RNA (siRNA) to knock down LXRs. siRNA-mediated knockdown of LXR $\alpha$ , but not LXR $\beta$ , increased UCP1 protein expression in T-brites, indicating that LXR $\beta$  does not regulate UCP1 expression and also may not compensate for LXR $\alpha$  (Figure S10B). Moreover, uncoupled respiration was increased in LXR $\alpha$ -, but not LXR $\beta$ -, depleted T-brites, independent of CIDEA (Figure S10C). Overall, our observations indicate that CIDEA affects UCP1 transcription via LXR $\alpha$ .

**CIDEA-LXR Dynamics Is Key to UCP1 Transcriptional Regulation**

To test whether CIDEA has any direct interaction with UCP1 enhancer region, we performed *in vitro* biotinylated-DNA pull-down assays coupled with immunoblots. As shown in Figure 5G, CIDEA did not bind the 150-bp UCP1 distal enhancer region (dUER<sub>150bp</sub>), nor the DR1 or DR4 oligonucleotides, even in the presence of the LXR $\alpha$  heterodimeric partner RXR $\alpha$  (Figure 5G; top blots). Subsequent assays were performed in the presence of RXR $\alpha$  and the LXR $\alpha$  agonist, T0901317. LXR $\alpha$  (Figure 5G; middle blots) and PPAR $\gamma$  (Figure 5G; lower blots) bound their cognate sequences as efficiently as they bound dUER<sub>150bp</sub>.

Streptavidin pull-down assays of biotinylated dUER<sub>150bp</sub>, DR4, or DR1 sequences did not recover any CIDEA in the presence of LXR $\alpha$  or PPAR $\gamma$  (Figure 5H, blue box), suggesting that CIDEA may not bind the enhancer via LXR $\alpha$  or PPAR $\gamma$ . Unlike cross-linking with Formaldehyde (Short cross-linking spacer arm, ~2 Å), cross-linking with Formaldehyde-EGS (long spacer arm, ~16.1 Å) revealed a transient interaction of CIDEA with DR4 (Figure 5H) but not with DR1 (Figure S10D, blue box). As a positive control, biotinylated DR4 and DR1 pulled down LXR $\alpha$  and PPAR $\gamma$ , respectively (Figures 5H and S10D). Interestingly, LXR $\alpha$  binding with its cognate DR4 element in dUER<sub>150bp</sub> was weakened with increasing CIDEA (Figure 5H, red box), but not BSA (Figure 5I), concentrations, demonstrating the CIDEA binding specificity for LXR $\alpha$ . CIDEA had no effect on PPAR $\gamma$  binding to DR1 (Figure S10D; red square). PPAR $\gamma$  and its ligand rosiglitazone did not affect CIDEA-mediated inhibition of LXR $\alpha$ -DR4 binding (Figure S10E). Overall, the above-mentioned results show that CIDEA interacts with LXR $\alpha$ , which weakens LXR $\alpha$  binding to DR4.

**CIDEA Directly Binds to LXR $\alpha$  and Weakens Its Binding to UCP1 Enhancer**

To further test that CIDEA weakens LXR $\alpha$  binding to DR4, we produced a single-nucleotide (T-G) mutation one nucleotide before the DR4 core sequence, resulting in an AatII restriction site outside of DR4

(Figure 6A). The idea was that LXR $\alpha$  binding to DR4 would inhibit the cleavage with AatII restriction enzyme. As expected, in the absence of LXR $\alpha$ , there was a cleavage with AatII restriction enzyme, which was otherwise blocked by LXR $\alpha$  binding (Figure 6B). Interestingly, when this construct was incubated with LXR $\alpha$ , AatII cleavage of DR4 increased with increasing concentrations of CIDEA (Figure 6B; top left blot); this cleavage was unaffected by BSA (negative control; Figure 6B; bottom blot). Furthermore, the mutant DR4 fragment did not bind LXR $\alpha$  and was cleaved completely, even in the presence of LXR $\alpha$ , indicating that LXR $\alpha$  protects the DR4 element from cleavage (Figure 6B; top right blot). To further confirm, pull-down assays of nuclear lysates followed by LXR $\alpha$  and CIDEA immunoblots showed that CIDEA<sup>-/-</sup> T-brites recovered more LXR $\alpha$  than CIDEA<sup>+/+</sup> T-brites (Figure 6C) and that this increase was suppressed upon CIDEA re-expression (Figure 6C; far right lane). These results confirmed that CIDEA binding to LXR $\alpha$  results in its removal from the UCP1 enhancer releasing LXR $\alpha$  inhibition of UCP1 transcription. On the other hand, PPAR $\gamma$  recovery was reduced in CIDEA<sup>-/-</sup> T-brites but recovered upon re-expression of CIDEA (Figure 6C), suggesting that CIDEA positively regulates PPAR $\gamma$  binding to the UCP1 enhancer.

A previous study reported that CIDEA interacts with liver X receptors in white fat cells (Kulyte et al., 2011). We studied if there is a direct interaction of CIDEA with LXR $\alpha$  in brite adipocytes. Bidirectional co-immunoprecipitation (coIP) of CIDEA with LXR $\alpha$  (Figure 6D) suggested a physical interaction between these two proteins. Addition of the LXR ligand increased CIDEA coIP with LXR $\alpha$ , without any effect on LXR $\alpha$  IP (Figure 6D).

*In vitro* transcription and translation (IVTT)-coupled coIP immunoblot assays confirmed direct interaction of CIDEA with LXR $\alpha$  (Figure 6D); GFP did not bind either protein. These results showed that CIDEA interacts directly with LXR $\alpha$ . Furthermore, *in situ* proximity ligation assays (PLAs) demonstrated that CIDEA KO abolished the strong association between CIDEA and LXR (Figure 6E).

Based on the above-mentioned results, we then tested a hypothesis that increased CIDEA in the nucleus during browning of white adipocytes affects LXR $\alpha$  occupancy at the UCP1 enhancer. Indeed, ChIP-qPCR for LXR $\alpha$  showed decreased recovery of UCP1 enhancer-associated LXR $\alpha$  over the 2 days following induction of browning, in CIDEA<sup>+/+</sup> (Figure 6F) but not CIDEA<sup>-/-</sup> cells (Figure 6G). Similar results were obtained in the presence of LXR ligand (Figure S11A). CIDEA re-expression reduced LXR association with the UCP1 enhancer within 24 h in CIDEA<sup>-/-</sup> cells (Figure 6H), and this LXR $\alpha$  association with the enhancer recovered as the transient ectopic CIDEA re-expression subsided with time (Figures 6H and 1D).

Analysis of the UCP1 promoter-enhancer suggested six additional putative LXR response elements (Figure S11B) (Hong and Tontonoz, 2014). Functionality testing showed that, other than DR4 at -3,903, none of these were critical for LXR $\alpha$  binding of the UCP1 promoter-enhancer (Figure S11C).

Since LXR $\alpha$  is known to control a variety of genes in metabolic organs, we next studied if CIDEA-LXR $\alpha$  specifically regulates UCP1. We performed qRT-PCR and ChIP analysis on LXR $\alpha$ -regulated genes in T-brite adipocytes  $\pm$  CIDEA (Figure S12A). As shown in Figure S12B, except for GLUT4 and APOD none of the LXR-regulated genes showed any significant effect of CIDEA. This observation is in line with a study showing increase in GLUT4 expression in human brown adipocytes along with UCP1 and CIDEA, which makes human brown adipocytes more glucose responsive (Lee et al., 2016).

## DISCUSSION

Various studies have shown a positive association of CIDEA expression with healthy metabolic phenotype in humans (Dahlman et al., 2005; Feldo et al., 2013; Gummesson et al., 2007; Nordstrom et al., 2005; Puri et al., 2008; Wu et al., 2013; Zhang et al., 2008). Our present study deciphers a comprehensive cellular and molecular mechanism of CIDEA in the regulation of improved metabolism via regulating thermogenesis and browning by transcriptional regulation of UCP1 in humans (Figure 6I). Our results show that LXR $\alpha$  is the functional interactor of CIDEA, whereby CIDEA represses its activity on UCP1 enhancer. In this work, we first developed dual-RNA based CRISPR-Cas9 and modified-RNA methodologies to modulate CIDEA expression efficiently in cultured human primary adipocytes derived from hADSCs. The T-brite phenotype was confirmed by heightened thermogenic capacity and expression of brite/beige adipocyte markers (Kajimura et al., 2015). Importantly, our experiments demonstrated that CIDEA leads to browning of human adipocytes via transcriptional regulation of UCP1, wherein CIDEA interacts directly with LXR $\alpha$ , thereby weakening LXR $\alpha$  binding to the UCP1 enhancer. Our results were supported by a previous study that

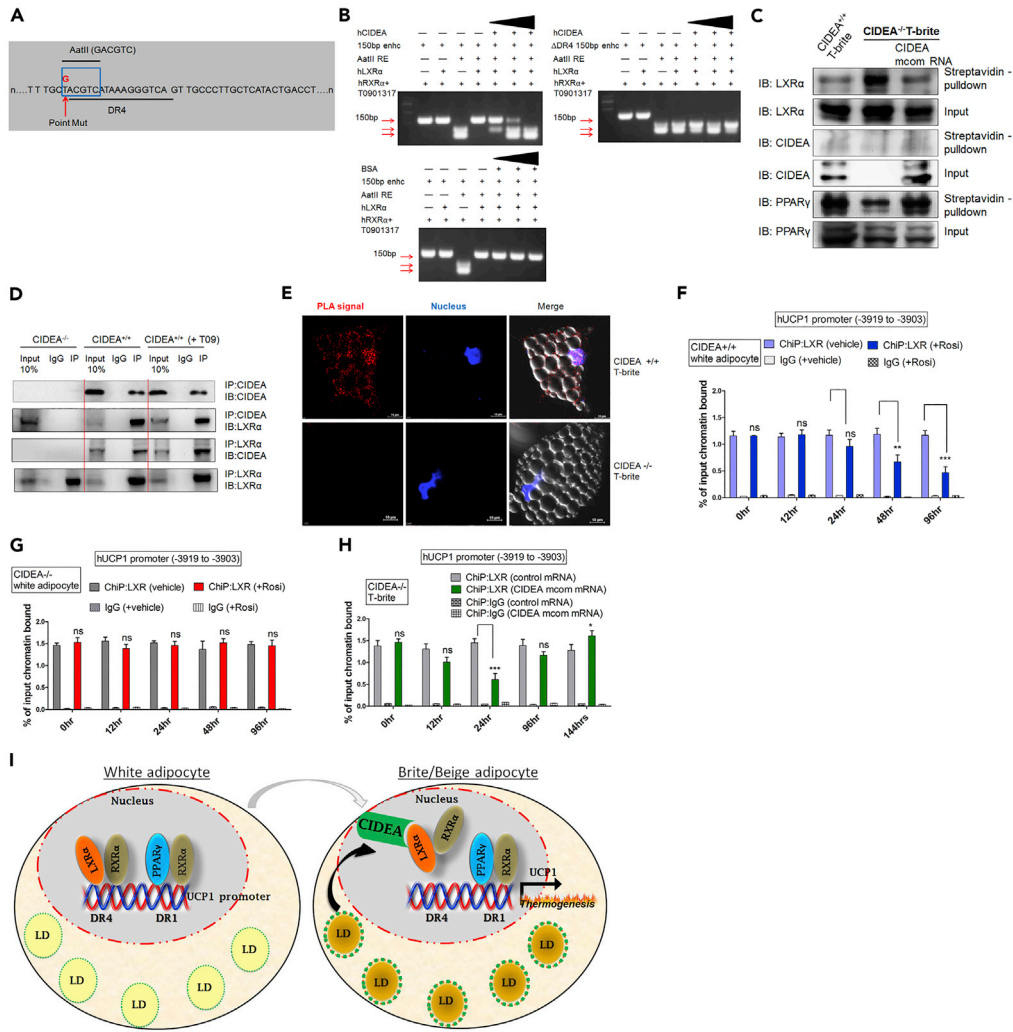


**Figure 6. CIDEA Directly Binds to LXR $\alpha$  to Derepress UCP1 Transcription during Britening**

(A) Partial sequence of the WT *UCP1* enhancer containing DR4 (LXR $\alpha$  binding site). T-G (red) point mutation (blue box) flanking DR4 that generated an artificial AatII restriction site. It did not alter LXR $\alpha$  binding to DR4 (data not shown).

(B) RFLP-based protein-DNA binding assay showing that LXR $\alpha$  protects synthetic AatII restriction site (lane 4, top left panel). CIDEA increased AatII cleavage efficiency dose dependently (lanes 5–7, top right panel); BSA (negative control) did not stimulate AatII cleavage (lanes 5–7, bottom panel).

(C) LXR and CIDEA immunoblots of streptavidin pull-down assays of nuclear fractions that had been incubated with biotinylated dUER<sub>150bp</sub> containing DR4.

(D) CIDEA and LXR $\alpha$  colP and western blots of total cell (20 kDa cutoff) lysate (input) from CIDEA KO, WT, and WT + T09 LXR ligand T-brites.

(E) PLA of CIDEA-LXR $\alpha$  protein-protein interaction in fixed WT T-brites (proteins detected with anti-CIDEA and anti-LXR $\alpha$  antibodies; CIDEA-LXR $\alpha$  interactions within 30–40 nm appear red; blue, Hoechst nuclear counterstain; LDs appear as glossy intracellular globes). Scale bar, 10  $\mu$ m.

(F and G) ChIP-qPCR analysis of LXR $\alpha$  binding to *UCP1* enhancer at –3,919 during Rosi-induced britening of CIDEA<sup>+/+</sup> (F) or CIDEA<sup>-/-</sup> (G) adipocytes.

(H) Time course ChIP-qPCR analysis of hUCP1 enhancer occupancy at –3,919 by LXR $\alpha$  in developing CIDEA<sup>-/-</sup> T-brites in which mcom-CIDEA mRNA transfection commenced concomitantly with Rosi induction.

(I) Model: Upon induction of human adipocyte britening, increasing concentrations of CIDEA result in CIDEA shuttling to the nucleus, where it interacts directly with LXR $\alpha$  and weakens LXR $\alpha$  binding of the *UCP1* enhancer at DR4, thus increasing transcriptional regulation of *UCP1* and thermogenesis.

In (F–H), data are mean  $\pm$  SEM (n = 3). \*\*\*p < 0.001, and \*\*p < .01, two-way ANOVAs followed by Bonferroni post-tests.

showed that CIDEA binds to LXRs and regulates their activity in human white adipocytes (Kulyte et al., 2011). Also, the propensity for UCP1 induction in human adipocytes has been shown to be correlated with CIDEA levels and withdrawal of thermogenic induction led rapidly to instability of CIDEA protein and UCP1 mRNA *in vivo* (Rosenwald et al., 2013) and *in vitro* (data not shown). Reintroducing CIDEA into CIDEA<sup>-/-</sup> cells rescued fully functional T-brite formation, as well as a correlation between CIDEA levels and increased UCP1 transcription and activity. This work defines a crucial role of CIDEA in regulating the brite phenotype in human adipocytes.

In rodents, UCP1 transcription is regulated largely by a combined effect of the CRE<sub>1</sub> proximal segment and a strong enhancer region ~2.5 kb upstream of the transcription start site; in humans, this region is ~3.9 kb upstream of the transcription start site. Additionally, the human proximal promoter region has more CpG islands than in the mouse (human ENCOD database). Our analysis showed that a 150-bp distal enhancer region (-4,000 to -3,058) of human UCP1 is DNase 1 hypersensitive, indicating multiple transcription factor-binding sites and suggesting that the mechanisms regulating UCP1 transcription may differ between humans and mice. In fact, ISO-mediated UCP1 transcription is weaker in humans than in rodents (del Mar Gonzalez-Barroso et al., 2000). Surprisingly, CIDEA regulation of UCP1 was indirect via a long loop interaction with LXR $\alpha$ . Although CIDEA interacts physically with both LXR $\alpha$  and LXR $\beta$  (data not shown), our data indicate that only CIDEA-LXR $\alpha$  interactions are crucial for UCP1 transcription, perhaps owing to its relatively greater stability. It is possible that CIDEA might remove LXR $\alpha$  from DR4, thereby helping PPAR $\gamma$  to regain control over limiting amounts of RXR $\alpha$ , a heterodimeric partner crucial for LXR $\alpha$  and PPAR $\gamma$  activity.

During adipocyte briteing, CIDEA was shuttled to the nucleus via its bipartite NLS, independent of active transport and the classical  $\alpha/\beta$  importin pathway. Notably, we incorporated HA tags into the mutants to keep the CIDEA molecule small enough for passive diffusion (Timney et al., 2016). We hypothesize that specific amino acids in the bipartite NLS may interact with nuclear pore proteins during passive diffusion to overcome a steep concentration gradient. These nuclear pore proteins may influence the passive diffusion rate.

CIDEA knockout mice were reported to have a lean phenotype and resistance to diet-induced obesity. It was explained on the basis of reduced UCP1 activity by CIDEA by physically interacting with it in mitochondria (Wu et al., 2014), although later studies showed that CIDEA is not localized in adipocyte mitochondria (Christianson et al., 2010; Puri et al., 2008; Wang et al., 2012). These seemingly disparate results in CIDEA function might also be due to increased lipolysis in whole-body CIDEA-knockout mouse, which produces excessive intracellular FFAs that might cause increased respiration through non-specific protonophoric FFA actions and PTP opening (Li et al., 2014) resulting in increased thermogenicity. A recent study showed that, in adipose-specific CIDEA transgenic mouse, CIDEA adipose expression is proportional to tissue briteing and UCP1 expression was increased owing to adipocyte hyper-recruitment from a mixed adipose tissue (Fischer et al., 2017). Given our observation that robust UCP1 expression precedes brite-adipocyte specific gene expression during briteing, we hypothesize that CIDEA-mediated de-repression of UCP1 could create mitochondrion-derived retrograde signaling to the nucleus for complete transdifferentiation of adipocytes into T-brites. It is also possible that inhibition of LXR $\alpha$  suppression by CIDEA could affect a broader network of genes, beyond UCP1, that drive adipocyte briteing. For example, our observation of reduced DIO2 (type II iodothyronine deiodinase) expression in CIDEA<sup>-/-</sup> adipocytes may be relevant for thermogenesis and briteing given that thyroid hormones have been linked with brown adipocyte formation and thermogenesis in mice via DIO2 upregulation (Weiner et al., 2016).

During thermogenic stimulation by PPAR $\gamma$  or cAMP (Chen et al., 2013), LXR $\alpha$  is recruited to the UCP1 enhancer (Wang et al., 2008). Our study showed that both of these conditions augmented CIDEA expression and CIDEA enrichment in the nucleus. It is notable that UCP1 transcription was decreased by nearly half but not completely abolished in our CIDEA<sup>-/-</sup> cells. Potential explanations for this remaining UCP1 transcription include initial dismissal of LXR $\alpha$  by PPAR $\gamma$  enabling basal UCP1 transcription, CRE downstream of the PPAR response element activating UCP1 transcription, and/or Rosi initiating a PPAR $\gamma$ -independent B38/mitogen-activated protein kinase phosphorylation cascade. Our time course ChIP analysis indicated that CIDEA was involved in the maintenance and robustness of UCP1 transcription, rather than its initiation, during adipocyte briteing.

CIDEA does not influence the chromatin retention of LXR $\alpha$  but rather interacts with it to alter its localized repressor activity on UCP1. Since CIDEA is a multifunctional protein, we performed a comprehensive

transcriptome analysis in brite human white adipocytes  $\pm$  CIDEA. As shown in Figure 3, UCP1 was the most upregulated gene in T-brite adipocytes. In conclusion, this study established a previously unidentified role of CIDEA in the transcriptional regulation of thermogenesis in human adipocytes and their briteing.

### Limitations of the Study

Our study defines the molecular role of CIDEA as a regulator of thermogenesis in human adipocytes. We have shown that CIDEA directly binds to LXR $\alpha$  and repress its activity on UCP1 enhancer. Although this study identified the role of CIDEA as a regulator of thermogenesis in human primary adipocytes, its *in vivo* role in humans remains to be proven. Presently, our results demonstrate that, during briteing of human adipocytes, CIDEA expression is increased resulting in translocation to the nucleus via a bipartite NLS. Future studies are required to identify the NLS-binding molecules that may facilitate the entry of CIDEA into the nucleus.

### METHODS

All methods can be found in the accompanying [Transparent Methods supplemental file](#).

### DATA AND CODE AVAILABILITY

The mRNA template sequences and their Gene Bank accession number is provided in the [Data S1](#) dataset file.

### SUPPLEMENTAL INFORMATION

Supplemental Information can be found online at <https://doi.org/10.1016/j.isci.2019.09.011>.

### ACKNOWLEDGMENTS

This work was supported by NIH/NIDDK grants DK101711 (VP) and R56DK094815 (VP). Dr. Puri received support through the Osteopathic Heritage Foundation's Vision 2020: Leading the Transformation of Primary Care in Ohio award to the Heritage College of Osteopathic Medicine at Ohio University.

### AUTHOR CONTRIBUTIONS

S.J. contributed to study design, performing experiments, analysis of results, and manuscript preparation. S.B. aided in experiments and manuscript preparation. M.-J.L. provided human tissue samples and contributed to data analysis. S.R.F. contributed to study design. V.P. contributed to study design and oversight, analysis of results, and manuscript preparation.

### DECLARATION OF INTERESTS

The authors declare no competing financial interests.

Received: May 3, 2019

Revised: August 2, 2019

Accepted: September 10, 2019

Published: October 25, 2019

### REFERENCES

- Abreu-Vieira, G., Fischer, A.W., Mattsson, C., de Jong, J.M., Shabalina, I.G., Ryden, M., Laurencikiene, J., Arner, P., Cannon, B., Nedergaard, J., et al. (2015). CIDEA improves the metabolic profile through expansion of adipose tissue. *Nat. Commun.* 6, 7433.
- Ahmadian, M., Abbott, M.J., Tang, T., Hudak, C.S., Kim, Y., Bruss, M., Hellerstein, M.K., Lee, H.Y., Samuel, V.T., Shulman, G.I., et al. (2011). Desnutrin/ATGL is regulated by AMPK and is required for a brown adipose phenotype. *Cell Metab.* 13, 739–748.
- Barneda, D., Frontini, A., Cinti, S., and Christian, M. (2013). Dynamic changes in lipid droplet-associated proteins in the "browning" of white adipose tissues. *Biochim. Biophys. Acta* 1831, 924–933.
- Barneda, D., Planas-Iglesias, J., Gaspar, M.L., Mohammadyani, D., Prasannan, S., Dormann, D., Han, G.S., Jesch, S.A., Carman, G.M., Kagan, V., et al. (2015). The brown adipocyte protein CIDEA promotes lipid droplet fusion via a phosphatidic acid-binding amphipathic helix. *Elife* 4, e07485.
- Bordicchia, M., Liu, D., Amri, E.Z., Ailhaud, G., Dessi-Fulgheri, P., Zhang, C., Takahashi, N., Sarzani, R., and Collins, S. (2012). Cardiac natriuretic peptides act via p38 MAPK to induce the brown fat thermogenic program in mouse and human adipocytes. *J. Clin. Invest.* 122, 1022–1036.
- Chen, H.Y., Liu, Q., Salter, A.M., and Lomax, M.A. (2013). Synergism between cAMP and PPARgamma signalling in the initiation of UCP1 gene expression in HIB1B brown Adipocytes. *PPAR Res.* 2013, 476049.
- Christianson, J.L., Boutet, E., Puri, V., Chawla, A., and Czech, M.P. (2010). Identification of the lipid droplet targeting domain of the CIDEA protein. *J. Lipid Res.* 51, 3455–3462.
- Dahlman, I., Kaaman, M., Jiao, H., Kere, J., Laakso, M., and Arner, P. (2005). The CIDEA gene

V115F polymorphism is associated with obesity in Swedish subjects. *Diabetes* 54, 3032–3034.

del Mar Gonzalez-Barroso, M., Pecqueur, C., Gelly, C., Sanchis, D., Alves-Guerra, M.C., Bouillaud, F., Ricquier, D., and Cassard-Doulcier, A.M. (2000). Transcriptional activation of the human *ucp1* gene in a rodent cell line. Synergism of retinoids, isoproterenol, and thiazolidinedione is mediated by a multipartite response element. *J. Biol. Chem.* 275, 31722–31732.

Feldo, M., Kocki, J., Lukasik, S., Bogucki, J., Feldo, J., Terlecki, P., Kesik, J., Wronski, J., and Zubilewicz, T. (2013). CIDEA gene expression in patients with abdominal obesity and LDL hyperlipoproteinemia qualified for surgical revascularization in chronic limb ischemia. *Pol. Przegl. Chir.* 85, 644–648.

Fischer, A.W., Shabalina, I.G., Mattsson, C.L., Abreu-Vieira, G., Cannon, B., Nedergaard, J., and Petrovic, N. (2017). UCP1 inhibition in CIDEA-overexpressing mice is physiologically counteracted by brown adipose tissue hyperrecruitment. *Am. J. Physiol. Endocrinol. Metab.* 312, E72–E87.

Fisher, F.M., Kleiner, S., Douris, N., Fox, E.C., Mepani, R.J., Verdegue, F., Wu, J., Kharitonov, A., Flier, J.S., Maratos-Flier, E., et al. (2012). FGF21 regulates PGC-1 $\alpha$  and browning of white adipose tissues in adaptive thermogenesis. *Genes Dev.* 26, 271–281.

Ghorbani, M., and Himms-Hagen, J. (1997). Appearance of brown adipocytes in white adipose tissue during CL 316,243-induced reversal of obesity and diabetes in Zucker *fa/fa* rats. *Int. J. Obes. Relat. Metab. Disord.* 21, 465–475.

Grahn, T.H., Kaur, R., Yin, J., Schweiger, M., Sharma, V.M., Lee, M.J., Ido, Y., Smas, C.M., Zechner, R., Lass, A., et al. (2014). Fat-specific protein 27 (FSP27) interacts with adipose triglyceride lipase (ATGL) to regulate lipolysis and insulin sensitivity in human adipocytes. *J. Biol. Chem.* 289, 12029–12039.

Granneman, J.G., Li, P., Zhu, Z., and Lu, Y. (2005). Metabolic and cellular plasticity in white adipose tissue I: effects of beta3-adrenergic receptor activation. *Am. J. Physiol. Endocrinol. Metab.* 289, E608–E616.

Gumesson, A., Jernas, M., Svensson, P.A., Larsson, I., Glad, C.A., Schele, R., Gripeteg, L., Sjöholm, K., Lystig, T.C., Sjöström, L., et al. (2007). Relations of adipose tissue CIDEA gene expression to basal metabolic rate, energy restriction, and obesity: population-based and dietary intervention studies. *J. Clin. Endocrinol. Metab.* 92, 4759–4765.

Harms, M., and Seale, P. (2013). Brown and beige fat: development, function and therapeutic potential. *Nat. Med.* 19, 1252–1263.

Hiraiki, Y., Waki, H., Yu, J., Nakamura, M., Miyake, K., Nagano, G., Nakaki, R., Suzuki, K., Kobayashi, H., Yamamoto, S., et al. (2017). NFIA co-localizes with PPAR $\gamma$  and transcriptionally controls the brown fat gene program. *Nat. Cell Biol.* 19, 1081–1092.

Hong, C., and Tontonoz, P. (2014). Liver X receptors in lipid metabolism: opportunities for

drug discovery. *Nat. Rev. Drug Discov.* 13, 433–444.

Juge-Aubry, C., Pernin, A., Favez, T., Burger, A.G., Wahli, W., Meier, C.A., and Desvergne, B. (1997). DNA binding properties of peroxisome proliferator-activated receptor subtypes on various natural peroxisome proliferator response elements. Importance of the 5'-flanking region. *J. Biol. Chem.* 272, 25252–25259.

Kajimura, S., Spiegelman, B.M., and Seale, P. (2015). Brown and beige fat: physiological roles beyond heat generation. *Cell Metab.* 22, 546–559.

Kazak, L., Chouchani, E.T., Jedrychowski, M.P., Erickson, B.K., Shinoda, K., Cohen, P., Vetrivelan, R., Lu, G.Z., Laznik-Bogoslavski, D., Hasenfuss, S.C., et al. (2015). A creatine-driven substrate cycle enhances energy expenditure and thermogenesis in beige fat. *Cell* 163, 643–655.

Kulyte, A., Pettersson, A.T., Antonson, P., Stenson, B.M., Langin, D., Gustafsson, J.A., Staels, B., Ryden, M., Arner, P., and Laurencikienė, J. (2011). CIDEA interacts with liver X receptors in white fat cells. *FEBS Lett.* 585, 744–748.

Laurencikienė, J., Stenson, B.M., Arvidsson Nordstrom, E., Agustsson, T., Langin, D., Isaksson, B., Permert, J., Ryden, M., and Arner, P. (2008). Evidence for an important role of CIDEA in human cancer cachexia. *Cancer Res.* 68, 9247–9254.

Lee, M.J., Pickering, R.T., and Puri, V. (2013). Prolonged Efficiency of siRNA-Mediated Gene Silencing in Primary Cultures of Human Preadipocytes and Adipocytes (Obesity).

Lee, M.J., Wu, Y., and Fried, S.K. (2012). A Modified Protocol to Maximize Differentiation of Human Preadipocytes and Improve Metabolic Phenotypes (Obesity).

Lee, P., Bova, R., Schofield, L., Bryant, W., Dieckmann, W., Slattery, A., Govendir, M.A., Emmett, L., and Greenfield, J.R. (2016). Brown adipose tissue exhibits a glucose-responsive thermogenic biorhythm in humans. *Cell Metab.* 23, 602–609.

Li, Y., Fromme, T., Schweizer, S., Schottl, T., and Klingenspor, M. (2014). Taking control over intracellular fatty acid levels is essential for the analysis of thermogenic function in cultured primary brown and brite/beige adipocytes. *EMBO Rep.* 15, 1069–1076.

McDonald, M.E., Li, C., Bian, H., Smith, B.D., Layne, M.D., and Farmer, S.R. (2015). Myocardin-related transcription factor A regulates conversion of progenitors to beige adipocytes. *Cell* 160, 105–118.

Nedergaard, J., Bengtsson, T., and Cannon, B. (2007). Unexpected evidence for active brown adipose tissue in adult humans. *Am. J. Physiol. Endocrinol. Metab.* 293, E444–E452.

Nedergaard, J., and Cannon, B. (2010). The changed metabolic world with human brown adipose tissue: therapeutic visions. *Cell Metab.* 11, 268–272.

Nedergaard, J., and Cannon, B. (2013). How brown is brown fat? It depends where you look. *Nat. Med.* 19, 540–541.

Nordstrom, E.A., Ryden, M., Backlund, E.C., Dahlman, I., Kaaman, M., Blomqvist, L., Cannon, B., Nedergaard, J., and Arner, P. (2005). A human-specific role of cell death-inducing DFFA (DNA fragmentation factor- $\alpha$ )-like effector A (CIDEA) in adipocyte lipolysis and obesity. *Diabetes* 54, 1726–1734.

Ohno, H., Shinoda, K., Spiegelman, B.M., and Kajimura, S. (2012). PPAR $\gamma$  agonists induce a white-to-brown fat conversion through stabilization of PRDM16 protein. *Cell Metab.* 15, 395–404.

Puri, V., Konda, S., Ranjit, S., Aouadi, M., Chawla, A., Chouinard, M., Chakladar, A., and Czech, M.P. (2007). Fat-specific protein 27, a novel lipid droplet protein that enhances triglyceride storage. *J. Biol. Chem.* 282, 34213–34218.

Puri, V., Ranjit, S., Konda, S., Nicoloso, S.M., Straubhaar, J., Chawla, A., Chouinard, M., Lin, C., Burkart, A., Corvera, S., et al. (2008). Cidea is associated with lipid droplets and insulin sensitivity in humans. *Proc. Natl. Acad. Sci. U S A* 105, 7833–7838.

Qiang, L., Wang, L., Kon, N., Zhao, W., Lee, S., Zhang, Y., Rosenbaum, M., Zhao, Y., Gu, W., Farmer, S.R., et al. (2012). Brown remodeling of white adipose tissue by SirT1-dependent deacetylation of Ppargamma. *Cell* 150, 620–632.

Reynolds, T.H.t., Banerjee, S., Sharma, V.M., Donohue, J., Couldwell, S., Sosinsky, A., Frulla, A., Robinson, A., and Puri, V. (2015). Effects of a high fat diet and voluntary wheel running exercise on cidea and CIDEA expression in liver and adipose tissue of mice. *PLoS One* 10, e0130259.

Rosenwald, M., Perdikari, A., Rulicke, T., and Wolfrum, C. (2013). Bi-directional interconversion of brite and white adipocytes. *Nat. Cell Biol.* 15, 659–667.

Seale, P., Bjork, B., Yang, W., Kajimura, S., Chin, S., Kuang, S., Scime, A., Devarakonda, S., Conroe, H.M., Erdjument-Bromage, H., et al. (2008). PRDM16 controls a brown fat/skeletal muscle switch. *Nature* 454, 961–967.

Seale, P., Kajimura, S., Yang, W., Chin, S., Rohas, L.M., Uldry, M., Tavernier, G., Langin, D., and Spiegelman, B.M. (2007). Transcriptional control of brown fat determination by PRDM16. *Cell Metab.* 6, 38–54.

Singh, M., Kaur, R., Lee, M.J., Pickering, R.T., Sharma, V.M., Puri, V., and Kandror, K.V. (2014). Fat-specific protein 27 inhibits lipolysis by facilitating the inhibitory effect of transcription factor Egr1 on transcription of adipose triglyceride lipase. *J. Biol. Chem.* 289, 14481–14487.

Timney, B.L., Raveh, B., Mironska, R., Trivedi, J.M., Kim, S.J., Russel, D., Wenthe, S.R., Sali, A., and Rout, M.P. (2016). Simple rules for passive diffusion through the nuclear pore complex. *J. Cell Biol.* 215, 57–76.

Vernochet, C., McDonald, M.E., and Farmer, S.R. (2010). Brown adipose tissue: a promising target

to combat obesity. *Drug News Perspect.* 23, 409–417.

Vernochet, C., Peres, S.B., Davis, K.E., McDonald, M.E., Qiang, L., Wang, H., Scherer, P.E., and Farmer, S.R. (2009). C/EBPalpha and the corepressors CtBP1 and CtBP2 regulate repression of select visceral white adipose genes during induction of the brown phenotype in white adipocytes by peroxisome proliferator-activated receptor gamma agonists. *Mol. Cell Biol.* 29, 4714–4728.

Wang, H., Liu, L., Lin, J.Z., Aprahamian, T.R., and Farmer, S.R. (2016). Browning of white adipose tissue with Roscovitine induces a distinct population of UCP1+ Adipocytes. *Cell Metab.* 24, 835–847.

Wang, H., Zhang, Y., Yehuda-Shnaidman, E., Medvedev, A.V., Kumar, N., Daniel, K.W., Robidoux, J., Czech, M.P., Mangelsdorf, D.J., and

Collins, S. (2008). Liver X receptor alpha is a transcriptional repressor of the uncoupling protein 1 gene and the brown fat phenotype. *Mol. Cell Biol.* 28, 2187–2200.

Wang, W., Lv, N., Zhang, S., Shui, G., Qian, H., Zhang, J., Chen, Y., Ye, J., Xie, Y., Shen, Y., et al. (2012). CIDEA is an essential transcriptional coactivator regulating mammary gland secretion of milk lipids. *Nat. Med.* 18, 235–243.

Weiner, J., Kranz, M., Kloting, N., Kunath, A., Steinhoff, K., Rijntjes, E., Kohrle, J., Zeisig, V., Hankir, M., Gebhardt, C., et al. (2016). Thyroid hormone status defines brown adipose tissue activity and browning of white adipose tissues in mice. *Sci. Rep.* 6, 38124.

Wu, J., Zhang, L., Zhang, J., Dai, Y., Bian, L., Song, M., Russell, A., and Wang, W. (2013). The genetic contribution of CIDEA polymorphisms, haplotypes and loci interaction to obesity in a

Han Chinese population. *Mol. Biol. Rep.* 40, 5691–5699.

Wu, L., Zhou, L., Chen, C., Gong, J., Xu, L., Ye, J., Li, D., and Li, P. (2014). Cidea controls lipid droplet fusion and lipid storage in brown and white adipose tissue. *Sci. China Life Sci.* 57, 107–116.

Zhang, L., Miyaki, K., Nakayama, T., and Muramatsu, M. (2008). Cell death-inducing DNA fragmentation factor alpha-like effector A (CIDEA) gene V115F (G→T) polymorphism is associated with phenotypes of metabolic syndrome in Japanese men. *Metabolism* 57, 502–505.

Zhou, Z., Yon Toh, S., Chen, Z., Guo, K., Ng, C.P., Ponniah, S., Lin, S.C., Hong, W., and Li, P. (2003). CIDEA-deficient mice have lean phenotype and are resistant to obesity. *Nat. Genet.* 35, 49–56.

**ISCI, Volume 20**

**Supplemental Information**

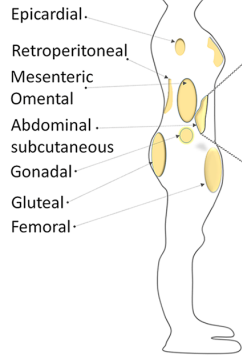
**CIDEA Transcriptionally Regulates UCP1  
for Britening and Thermogenesis  
in Human Fat Cells**

**Sukanta Jash, Sayani Banerjee, Mi-Jeong Lee, Stephen R. Farmer, and Vishwajeet Puri**

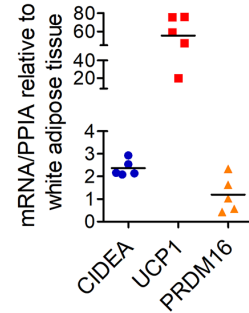
# SUPPLEMENTAL DATA

**a**

**Adipose depots**



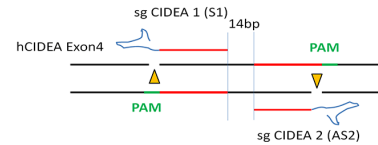
Patient	Age	Sex	Ethnicity	BMI
1	26	F	Caucasian	49
2	35	M	Caucasian	53
3	33	F	Hispanic	43
4	29	F	Hispanic	45
5	42	F	Caucasian	38



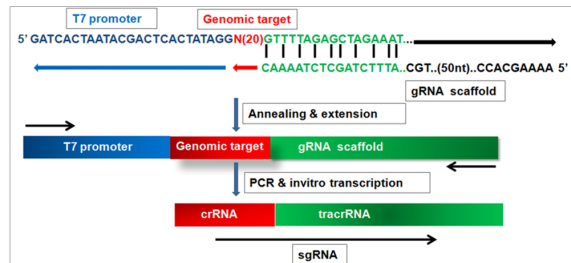
**b**

**CIDEA: Exon 4**

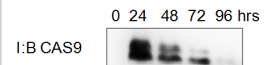
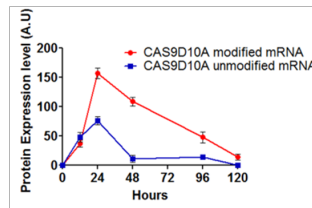
Break site ↓  
 5' GGCAGCCAGCAGCTCCCACTTGCTCGCCGCCGAAGAGTCTGGGAATAGCGAGAGTACACCTTCGACTTGTACAGGC 472  
 3' CCGTCGGTCGTGCAGGGTGAAAGAGCGCGGCTTCTCAGCCCTATCGCTCTCAGTGAAGCTGAACATGTCCG  
 Break site ↑



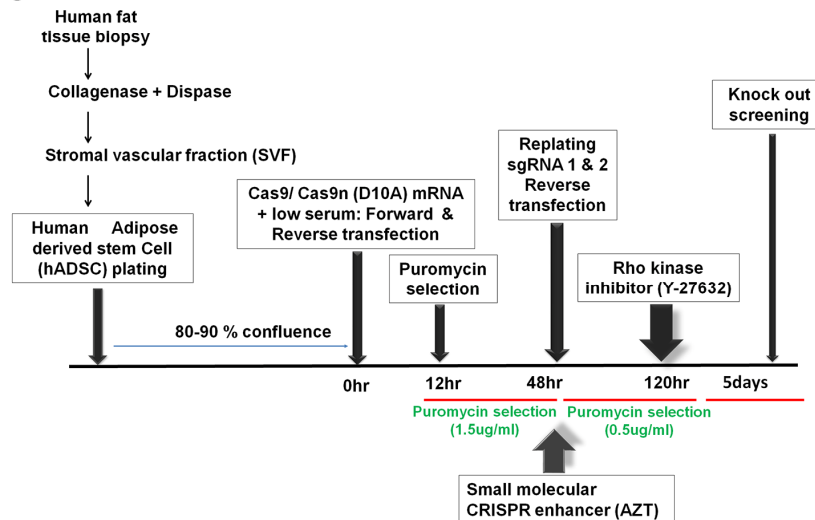
**c**



**d**

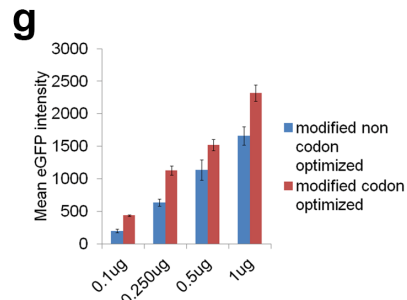
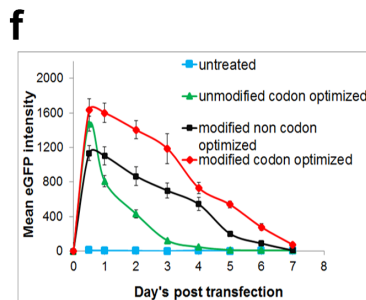
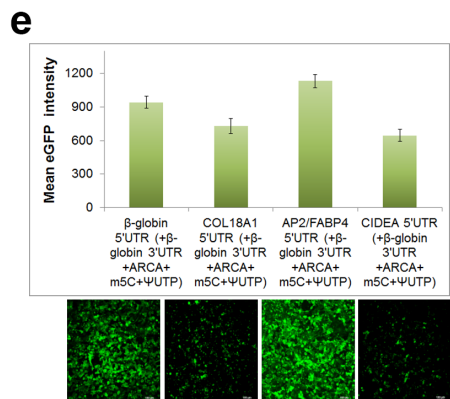
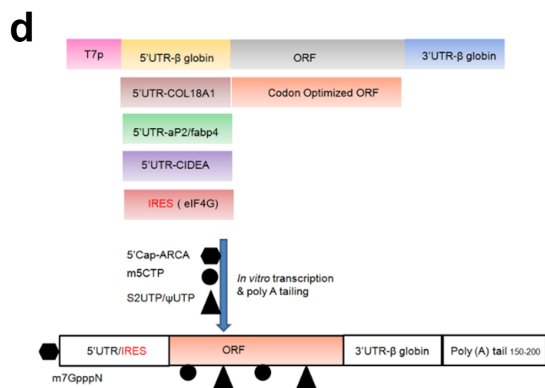
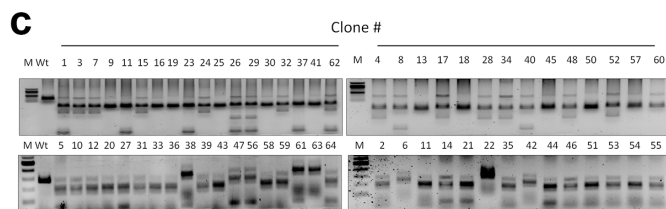
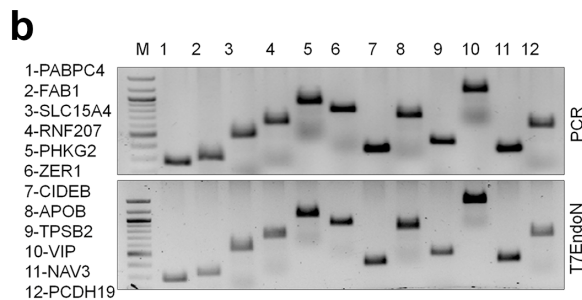
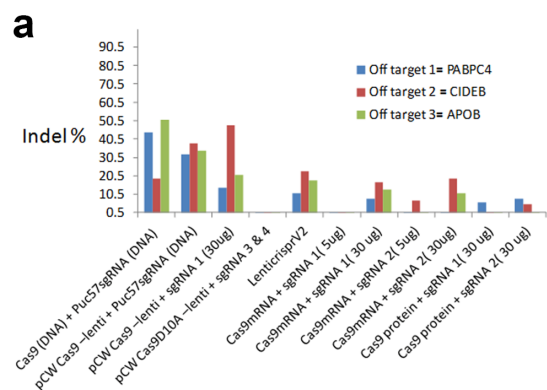


**e**

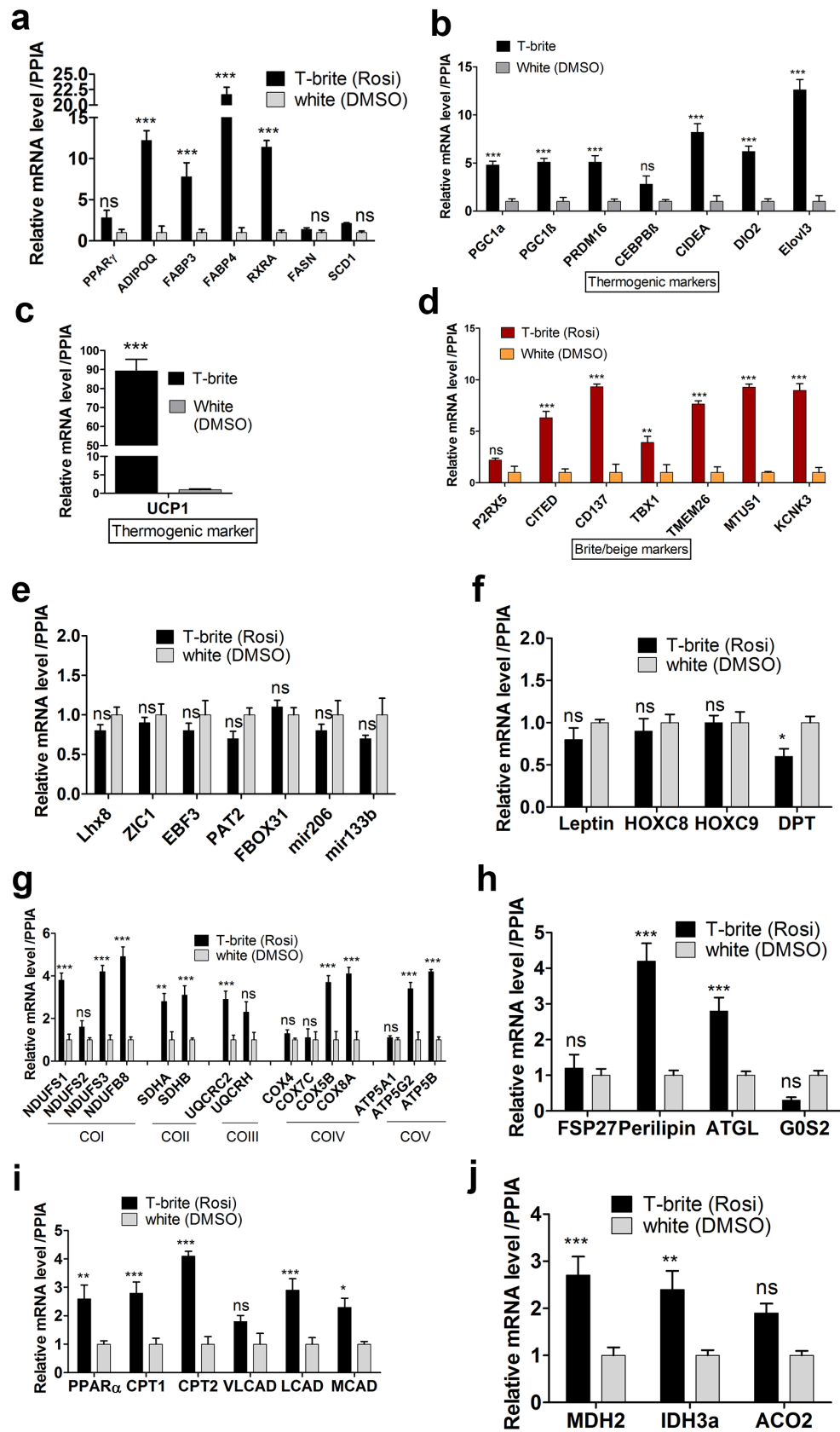


Jash et al., Figure S1

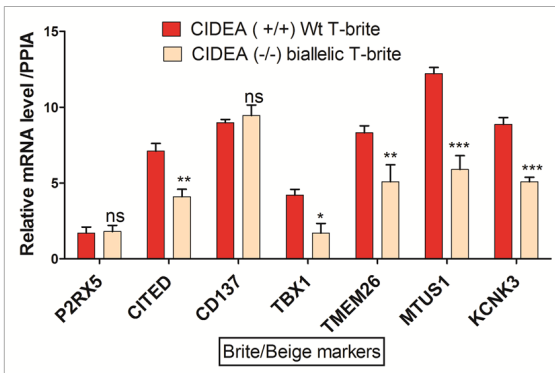
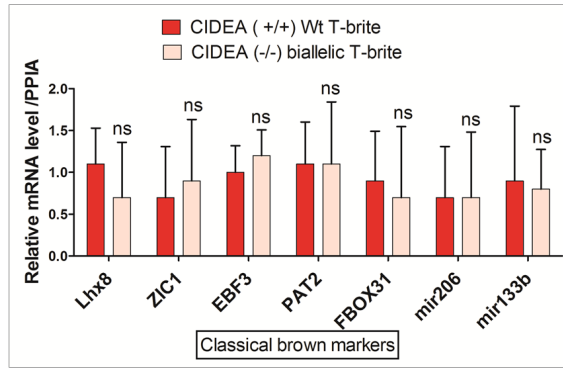
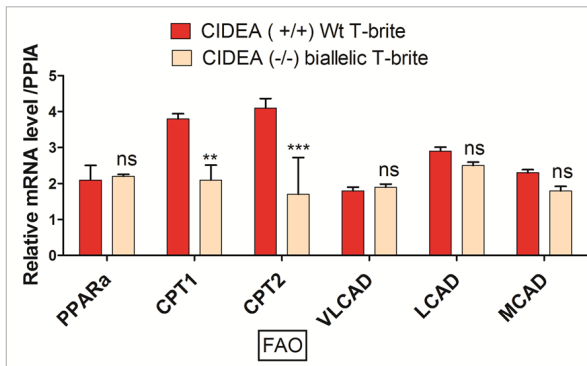
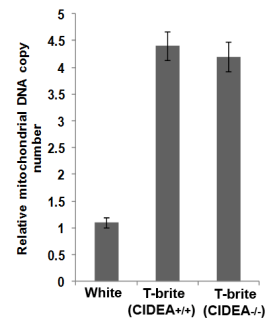
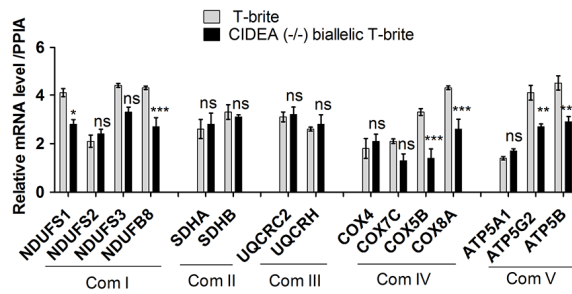




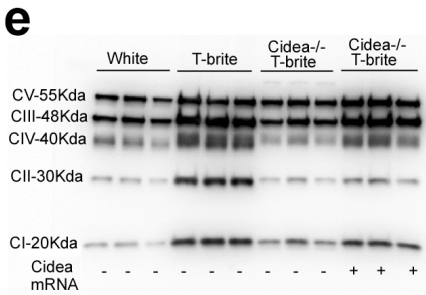
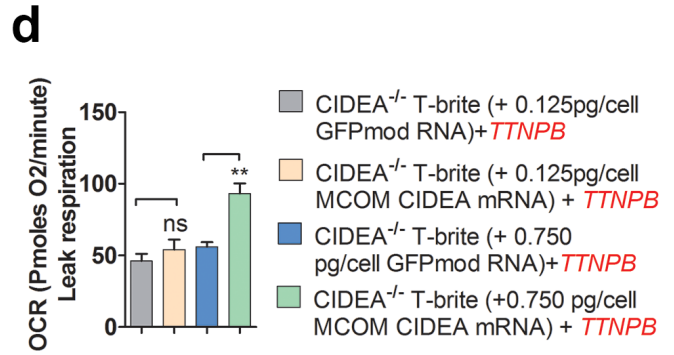
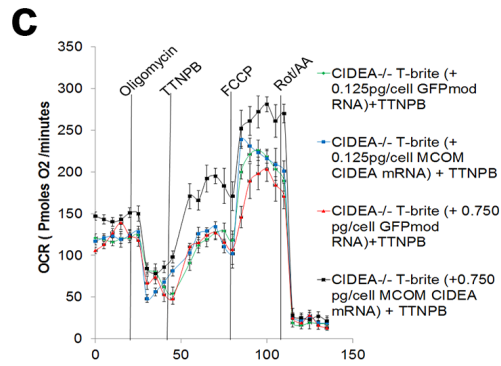
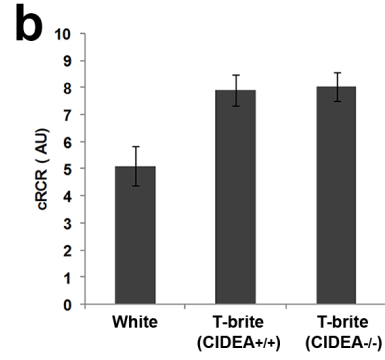
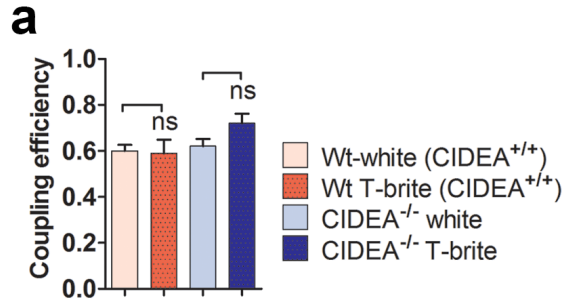
Jash et al., Figure S3



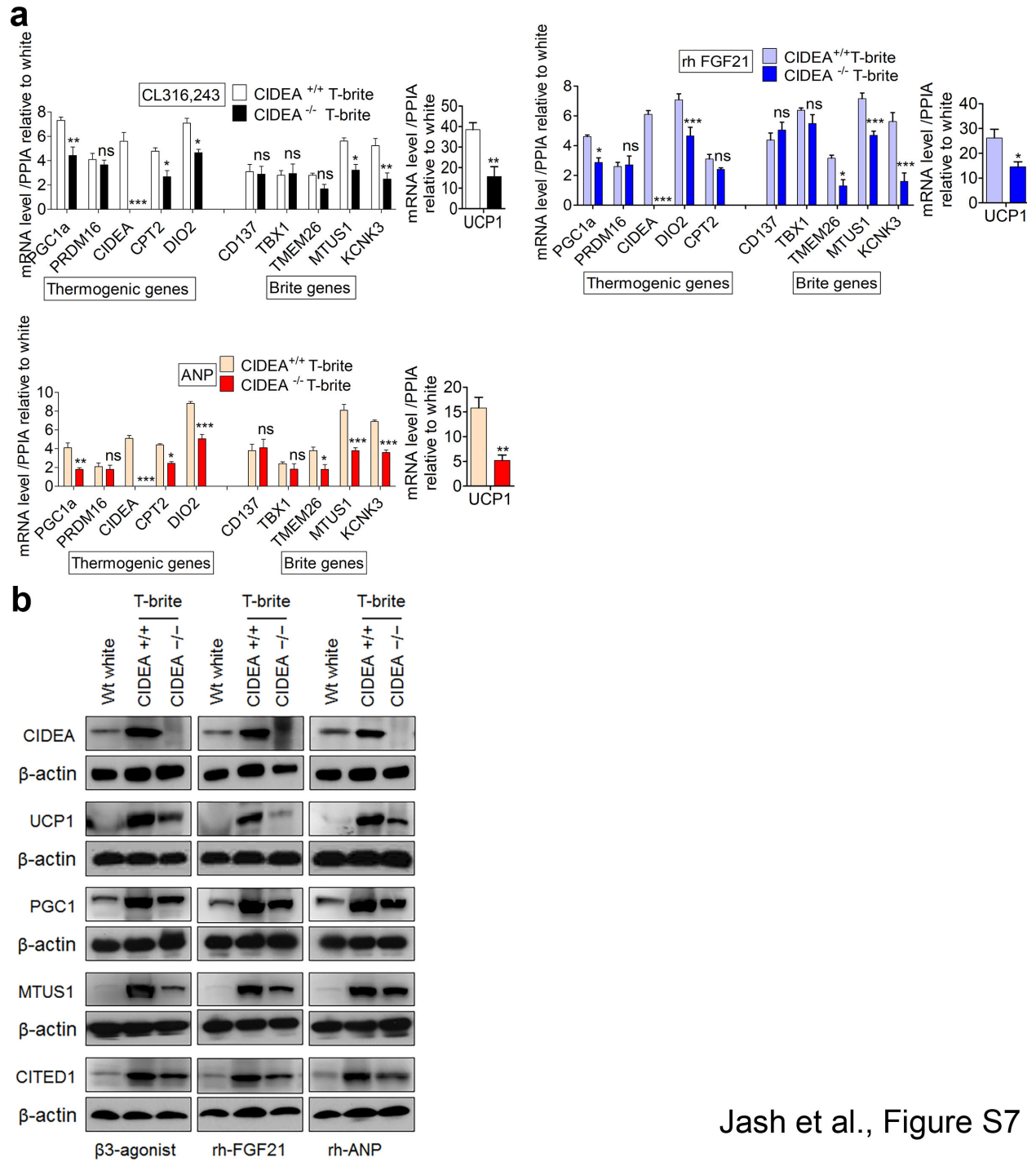
Jash et al., Figure S4

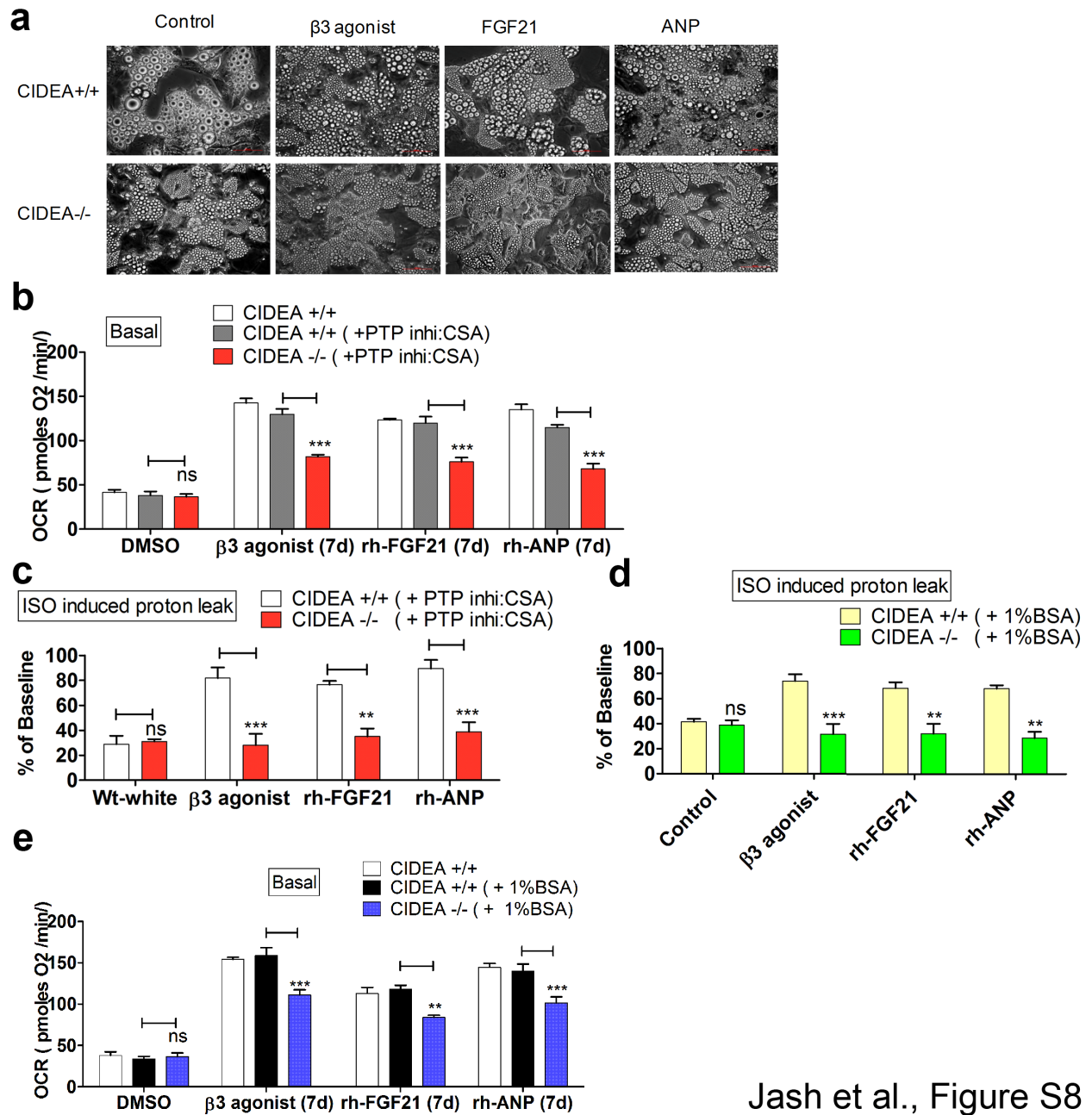
**a****b****c****d****e**

Jash et al., Figure S5

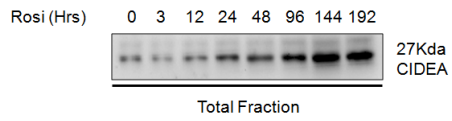
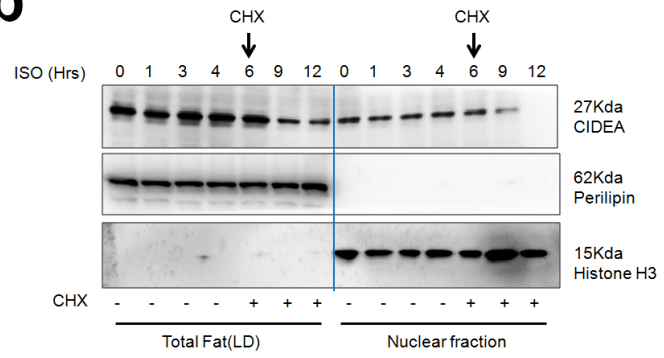
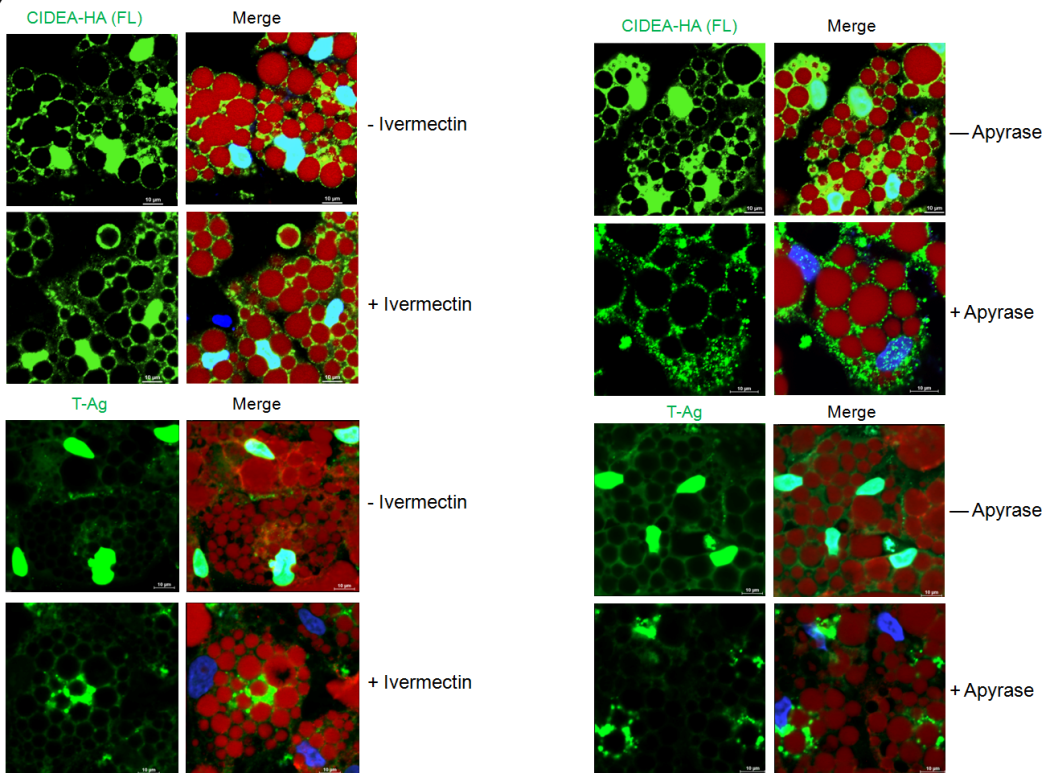


Jash et al., Figure S6

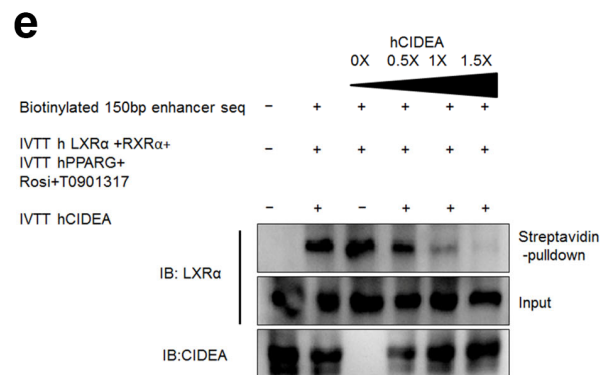
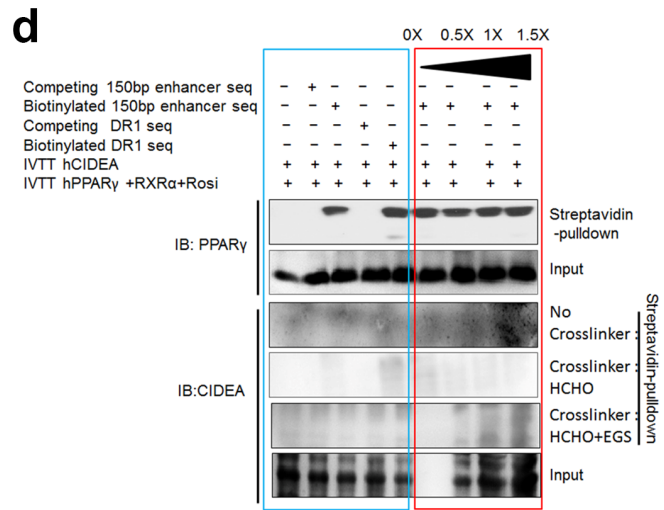
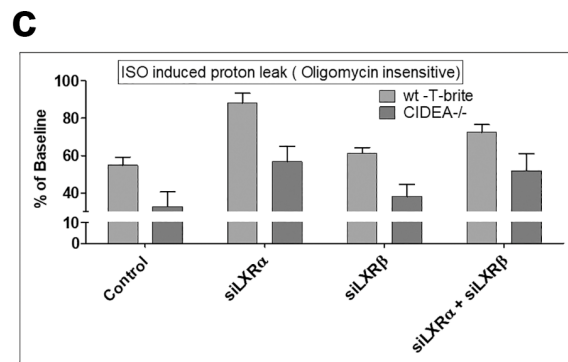
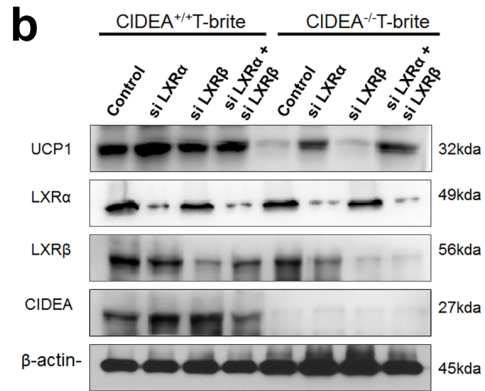
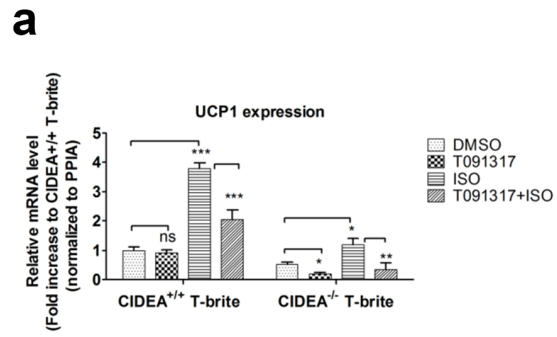




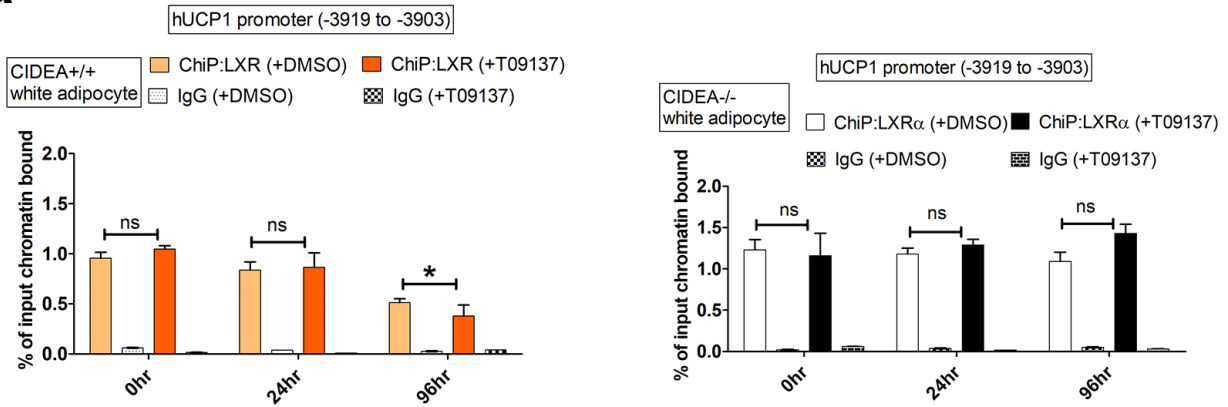
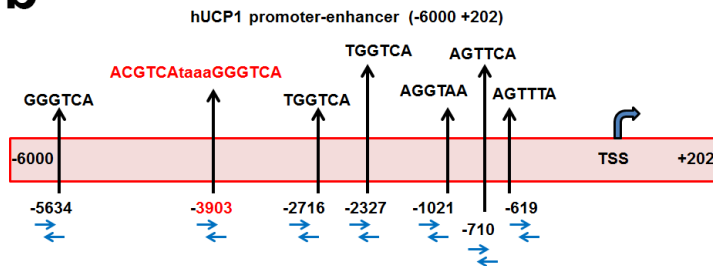
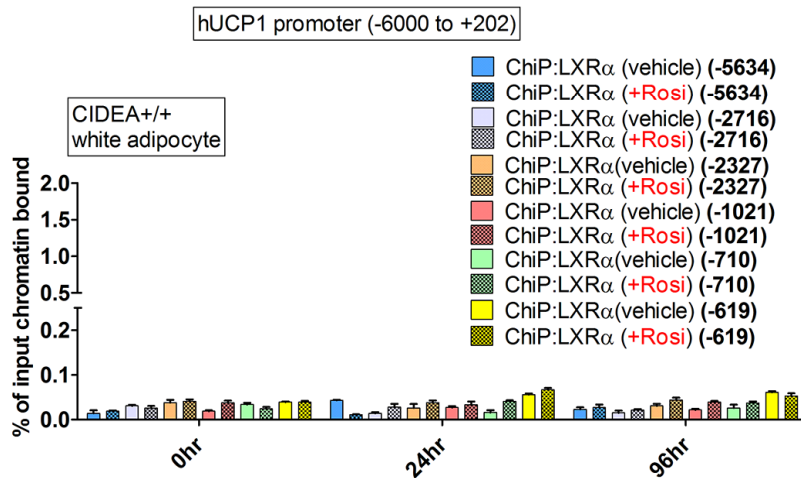
Jash et al., Figure S8

**a****b****c**

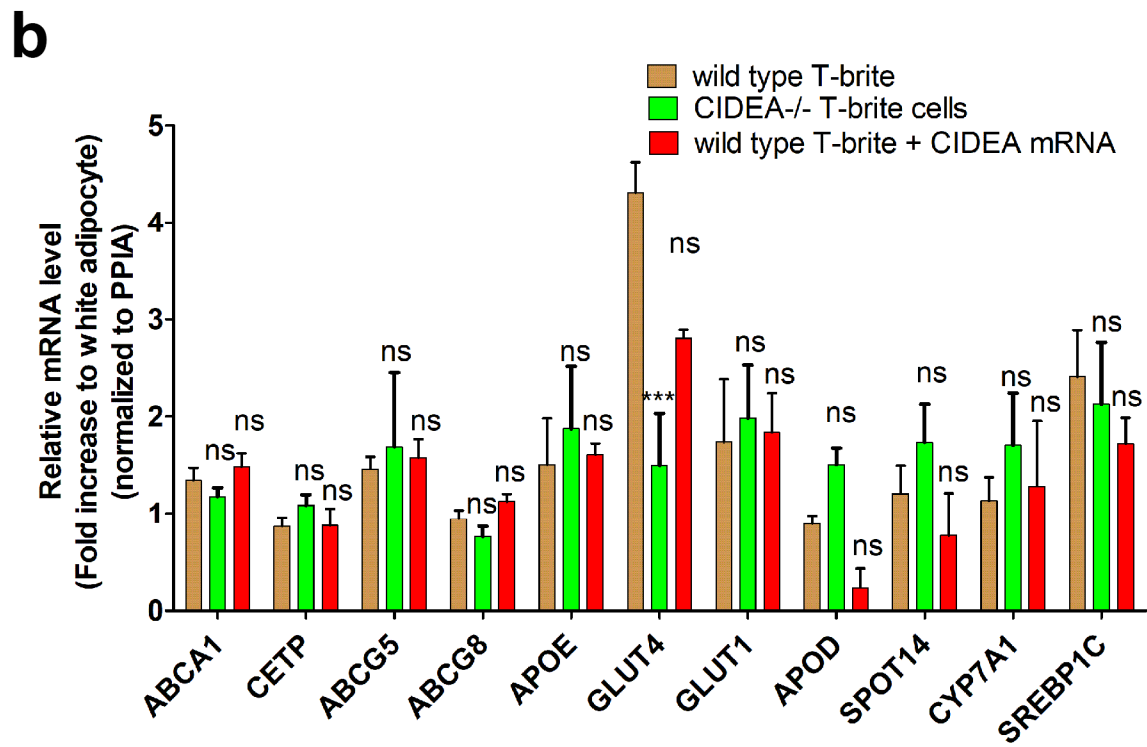
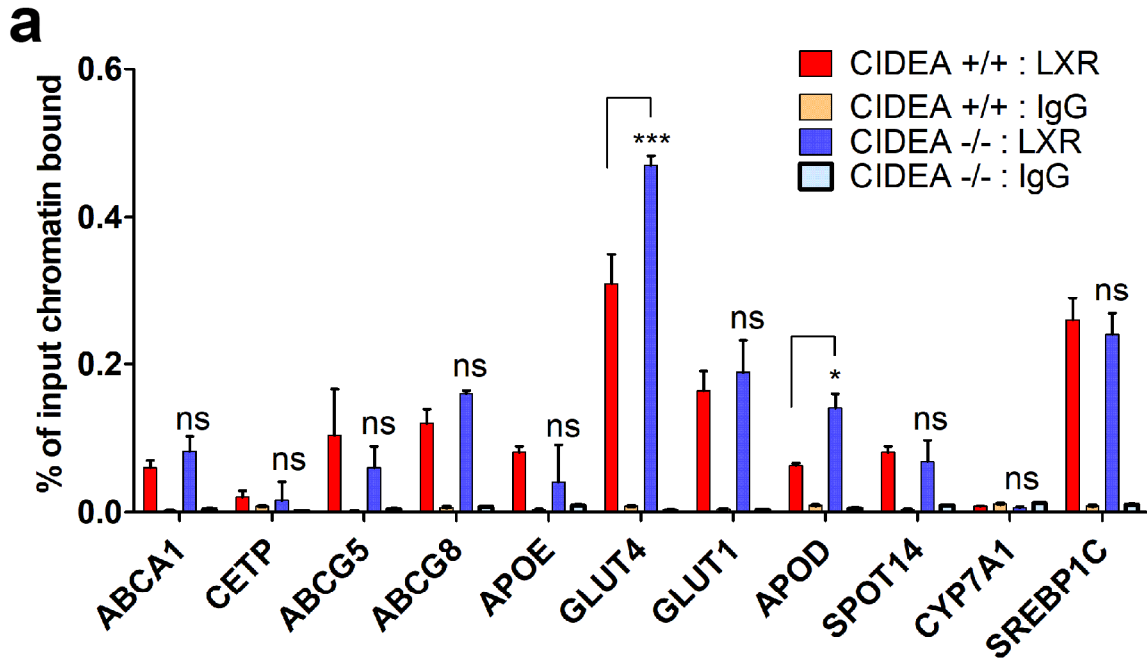
Jash et al., Figure S9



Jash et al., Figure S10

**a****b****c**

Jash et al, Figure S11



Jash et al., Figure S12

## SUPPLEMENTARY FIGURE LEGENDS

**Figure S1, Related to Figure 1. Construction and synthesis of CRISPR-Cas9 for targeting hCIDEA.** (a) Origin of subcutaneous adipose explants from five obese human subjects (left); induction of CIDEA and UCP1 with 1  $\mu$ M Rosi for 7 d (right). (b) Top: hCIDEA exon 4 targeted by S (sgRNA2) and AS (sgRNA1) sgRNA for double nicking; target sites are highlighted in green (sgRNA1) and blue (sgRNA2), and PAMs are underlined (red). Bottom: sgRNA binding and 14-bp offset between S and AS sgRNAs for efficient targeting and double nicking. (c) Hybridization of the T7 promoter-containing sgRNA oligo template and sgRNA scaffold template followed by template purification and *in vitro* transcription of the sgRNA template with modified nts. (d) Left: Time course of modified and unmodified Cas9D10A expression in human preadipocytes after Cas9D10A transfection. Data are mean  $\pm$  SEM (n = 3). Right: Western blot showing Cas9 expression. (e) Schematic workflow of CRISPR-Cas9D10A nickase-mediated CIDEA KO generation in primary human preadipocytes.

**Figure S2, Related to Figure 1. Developing CRISPR-Cas9nD10A for CIDEA KO.** (a) Titration of mod S and AS sgRNAs targeting hCIDEA- and Cas9D10A-mod mRNA for double nickase analysis. Y-axis shows insertion/deletion (indel) frequencies. Five off-target sites homologous for each CIDEA sgRNA were chosen based on mismatched nt positions. (b) Titration of S and AS sgRNAs targeting hCIDEA and Cas9D10A mod mRNA for evaluation of double nicking efficiency. Indel frequencies were determined with T7EndoN assays (each datum represents 3 separate experiments). (c) Double stranded break-specific nuclear localization of phosphorylated  $\gamma$ H2A.X in hADSCs showing efficiency of dual RNA-mediated CRISPR-Cas9

nickase. **(d)** mutation patterns detected by PCR amplification and Sanger sequencing. Wt, clones without indels. BA-Het, clones with biallelic heterogenous indel mutations in both alleles. BA-Homo, clones with biallelic homogenous indel mutations in both alleles (sgRNA1 and sgRNA2 target sites are in blue and green, respectively; PAM sites are underlined red). Dotted line, deletions; lower case orange letters, inserted sequences. Deleted ( $\Delta$ ) and inserted (+) nucleotides identified by Sanger sequencing are indicated to the right of each allele. **(e)** Representative phase-contrast images showing smaller LDs in CIDEA<sup>-/-</sup> white adipocytes than in WT [CIDEA<sup>+/+</sup>(wt)] white adipocytes. Lower panels show morphometric analysis of the number and radius of lipid droplets, and biochemical quantification of basal lipolysis based on measurement of glycerol release after 2 hours. Results for lipid droplet number and radius are an average of at least 10 cells from the same cover slip and/or the same field in three independent experiments. Data are mean  $\pm$  SEM (n = 3). **(f)** mRNA levels of adipogenic markers in CIDEA<sup>+/+</sup> and CIDEA<sup>-/-</sup> adipocytes. Data are mean  $\pm$  SEM (n = 3). **(g)** S (n = 8) and AS (n = 6) sgRNA target sites assessed according to software prediction. Mismatch nts are indicated in red and PAM motifs are underlined.

**Figure S3, Related to Figure 1. Developing CRISPR-Cas9nD10A for CIDEA KO, and mod mRNA for CIDEA expression in human adipocytes. (a)** Off-target cleavage by Cas9 and Cas9D10A with A or AS sgRNAs alone or in combination. Note that there were no off-target effects with Cas9D10A. **(b)** Representative T7EndoN analysis of high-scoring off-targets. **(c)** T7EndoN analysis of human preadipocyte clones after CRISPR-Cas9 nickase-mediated CIDEA KO. **(d)** CIDEA constructs for generation of CIDEA mod mRNA by *in vitro* transcription. Note the different 5'UTRs used with the beta-globin 3'UTR. CIDEA ORF was optimized for human

codon usage. The identities and quantities of modified and unmodified nucleotides used are presented in the methods section. **(e)** Confocal microscopic expression analysis of mod GFP mRNA construct with different 5'UTRs after single transfection into mature adipocytes. The AP2/FABP4 5'UTR was used in our further analysis. We observed 85–90% transfection with mod green fluorescent protein (GFP) mRNA in mature adipocytes; GFP expression varied across 5'UTR types, with AP2 5'UTR yielding particularly strong ribosome binding and translatability. Data are mean  $\pm$  SEM (n = 3). **(f)** Confocal microscopic time-course expression analysis of GFP mRNA with or without modified nts and codon optimization after single transfection into mature human adipocytes. The expression and stability of mod GFP mRNA were improved by nt mod and codon optimization. In mature adipocytes, mod GFP was expressed within 3 h, peaked after 12–24 h, and declined to basal levels by 6–7 d. Data are mean  $\pm$  SEM (n = 3). **(g)** Dose-dependent GFP expression in mature adipocytes with and without codon optimization. Data are mean  $\pm$  SEM (n = 3).

**Figure S4, Related to Figure 1. Rosi-induced browning of human white adipocytes.**

hADSCs derived from subcutaneous abdominal adipose were differentiated and then treated with 1  $\mu$ M Rosi for 7 d. The y-axis shows the relative mRNA levels of **(a)** differentiation markers common to white and brite/beige, **(b)** brite/beige fat cell-selective genes, **(c)** UCP1 expression, **(d)** brite markers, **(e)** white adipose-selective genes, **(f)** brown markers, **(g)** mitochondrial oxidative phosphorylation genes, **(h)** major lipolytic genes, **(i)** FAO, and **(j)** TCA genes. Each datum represents a mean fold change  $\pm$  SEM (vs. DMSO-treated controls) of pooled fractions from three donors. \*\*\*P < .001, \*\*P < .01, and \*P < .05, two-way ANOVA followed by Bonferroni post-test.

**Figure S5, Related to Figure 1. CIDEA KO inhibits briteing and uncoupling in human adipocytes.** Real-time qPCR analysis of the differential expression of (a) brite markers, (b) brown markers, and (c) FAO-related genes in CIDEA<sup>+/+</sup> (identified as Wt) versus biallelic CIDEA<sup>-/-</sup> T-brites. Mean fold changes ± SEM (vs. DMSO-treated controls) of five independent experiments are shown. (d) Relative mitochondrial DNA copy number in T-brites was unaffected by KO of CIDEA (T-brite CIDEA<sup>-/-</sup>). Data are mean ± SEM (n = 3). (e) Expression of oxidative phosphorylation genes in WT CIDEA<sup>+/+</sup> versus CIDEA<sup>-/-</sup> T-brites. \*\*\*P < .001, \*\*P < .01, and \*P < .05, two-way (a–c) or one-way (e) ANOVA followed by Bonferroni multi-comparison tests.

**Figure S6, Related to Figure 2. CIDEA KO inhibits OCR in human white adipocytes.** (a) Quantification of coupling efficiency of the samples in Fig. 2e. Data are mean ± SEM (n = 3). (b) Cell respiratory control ratio (cRCR) in white adipocytes, CIDEA<sup>+/+</sup> and CIDEA<sup>-/-</sup> T-brites. Data are mean ± SEM (n = 3). (c) OCR increases following TTNPB (50 μm) treatment of CIDEA<sup>-/-</sup> T-brites transfected with control-GFP mRNA or mcom-CIDEA mRNA. (d) TTNPB-induced increase in CIDEA<sup>-/-</sup> T-brite leak respiration correlated with the amount of mcom CIDEA mRNA delivered. Data are mean ± SEM (n = 3). \*\*P < .01, two-way ANOVA followed by Bonferroni multi-comparison tests. (e) Relative levels of oxidative phosphorylation subunits (CV-α [Atp5B], CIII-core2 [UQCRC2], CII-30 [SDHB], CIV-II [CytC-OxII], CI-20 [NdufB8]) in WT and KO T-brites. After a 7-d Rosi treatment, CIDEA<sup>-/-</sup> adipocytes were transfected with 0.750 pg/cell mcom-CIDEA mRNA or GFP control mRNA for 3 d (last three lanes). For Seahorse experiments 24 well plates seeded with equal number of cells were used. After

completion of the oxygen consumption measurement, each well in every experiment was found to have 10-12  $\mu\text{g}$  total protein.

**Figure S7, Related to Figure 2. CIDEA is critical for human white adipocyte browning by various activators/inducers.** (a) Quantitative reverse transcriptase (qRT)-PCR analysis of thermogenic and browning markers following induction of human white adipocytes with  $\beta 3$ -agonist (CL 316,243), FGF21, and ANP in the presence or absence of CIDEA. UCP1 expression was reduced in CIDEA<sup>-/-</sup> T-brites. Data are expressed as mean ( $\pm$ SEM) of five independent experiments; \*\*\*P < .001, \*\*P < .01, and \*P < .05, two-way ANOVA followed by Bonferroni multi-comparison tests. (b) CIDEA, UCP1, PGC1 $\alpha$ , MTUS1, and CITED1 protein expression in T-brites following induction with various inducers in the presence or absence of CIDEA.

**Figure S8, Related to Figure 2. Browning of human adipocytes by different browning-inducers is CIDEA dependent.**

(a) Representative phase-contrast images of adipocytes browned by each of several activators/inducers in WT CIDEA<sup>+/+</sup> versus KO CIDEA<sup>-/-</sup> (KO conducted in preadipocytes before differentiation). (b) Basal respiration (OCR in pmoles O<sub>2</sub>/min), and (c) ISO-induced proton leak respiration (OCR as % baseline) of T-brites generated by different stimuli. Before OCR measurements, cells were pretreated with the PTP inhibitor CSA. (d) Iso-induced proton leak, and (e) basal OCR was reduced in CIDEA<sup>-/-</sup> versus CIDEA<sup>+/+</sup> T-brites; 1% BSA was added to quench excess FFA activity. In b,c,d and e, the results are mean  $\pm$  SEM of three independent experiments. \*\*\*P < .001 and \*\*P < .01, one-way ANOVA followed by Bonferroni multi-comparison tests.

**Figure S9, Related to Figure 4. Lipid droplet to nuclear shuttling of CIDEA.**

(a) Time courses of CIDEA protein expression in human white adipocytes after addition of 1  $\mu$ M Rosi. (b) Effect of cycloheximide (CHX) on the ISO-induced subcellular distribution and nuclear enrichment of CIDEA. (c) Confocal images of T-brites expressing CIDEA-HA or SV-40 T-Ag GFP-NLS showing that, after 24-h transfection, 6-h 50  $\mu$ M ivermectin treatment did not prevent CIDEA import, but blocked  $\alpha/\beta$  importin recognition of HA-t-Ag incorporated NLS, whereas 6-h apyrase (0.1 U/ml) reduced nuclear import of CIDEA.

**Figure S10, Related to Figure 5. CIDEA regulates UCP1 expression via LXR $\alpha$ .**

(a) The LXR ligand T091317, which did not alter mean ( $\pm$ SEM) UCP1 expression in WT T-brites not treated with ISO, reduced *UCP1* mRNA expression in CIDEA<sup>-/-</sup> T-brites and in ISO-treated WT and KO T-brites. \*\*\*P < .001, \*\*P < .01, and \*P < .05, two-way ANOVA followed by Bonferroni post-test. (b) Loss of UCP1 protein in CIDEA<sup>-/-</sup> T-brites was reversed by introduction of LXR $\alpha$  suppressing siRNA (with or without LXR $\beta$  siRNA). During individual knockdown, 50 nM siRNA concentration was used, whereas, during dual-knockdown 25 nM concentration of each siRNA species was used. Cellular lysates were pooled from T-brites generated from three donors. (c) effect of siRNA-mediated LXR $\alpha$  and/or LXR $\beta$  depletion on iso-induced proton leak in T-brite adipocytes  $\pm$ CIDEA. Data are mean  $\pm$  SEM (n = 3). (d) Protein-DNA binding analysis of recombinant hCIDEA with dUER<sub>150bp</sub> DNA, including DR4, in the presence of recombinant human PPAR $\gamma$  (hPPAR $\gamma$ ) and its heterodimeric partner RXR $\alpha$  (blue box). The hPPAR $\gamma$ -dUER<sub>150bp</sub> interaction strength was unaffected by CIDEA levels (red box). No CIDEA was recovered by streptavidin pull-down followed by western blotting, with or

without a crosslinker. (e) Analysis of LXR $\alpha$  and PPAR $\gamma$  proteins with dUER<sub>150bp</sub> DNA, which includes DR4 and DR1, in the presence of equimolar amounts of hCIDEA, hPPAR $\gamma$  and RXR $\alpha$ .

**Figure S11, Related to Figure 6. CIDEA interacts with LXR to regulate UCP1**

**transcription.** (a) ChIP-qPCR analysis of LXR $\alpha$  binding to UCP1 promoter-enhancer at -3919 during Rosi-induced briteening of CIDEA<sup>+/+</sup> (left) or CIDEA<sup>-/-</sup> (right) adipocytes in the presence of LXR ligand T09137. Data are mean  $\pm$  SEM (n = 3). (b) Schematic representation of the multiple LXR response elements in the human UCP1 promoter (-6000 to +201). Among seven possible response elements, only the one at -3903 mediates LXR $\alpha$  binding. The half site of each response element is indicated above and the positions of the ChIP primer pairs are indicated below. (c) Time-course ChIP-qPCR analysis of LXR $\alpha$  occupancy over six LXR response elements (site loci indicated within parentheses; site at -3909 not included) in the human *UCP1* enhancer during Rosi-mediated briteening Data are mean  $\pm$  SEM (n = 3).

**Figure S12, Related to Figure 6. ChIP analysis of LXR regulated genes in the presence and**

**absence of CIDEA.** (a) Effect of CIDEA on LXR-regulated genes in T-brite adipocytes. (b)

Real-time PCR analysis of LXR regulated genes in T-brite adipocytes  $\pm$  CIDEA. In both a and b,

Data are mean  $\pm$  SEM (n = 3). \*\*\*P < 0.001 and \*P < .05, two-way ANOVA followed by

Bonferroni post-tests.

**Data S1, Related to Figures 1-6. mRNA template sequences.**

**Data S2, Related to Figures 1-6 and S1-S12. Genes, Primer ID and sequences.** List of all the genes, their primer IDs, primer sequences used in the study.

## **TRANSPARENT METHODS**

**Human subjects.** Adipose tissues were obtained from five human patients (mean age 48.6 years and BMI 34.6 kg/m<sup>2</sup>) during panniculectomy following weight loss. All subjects provided informed consent for participation. The protocol was approved by Institutional Review Board of Boston University Medical Center.

**Isolation of hADSCs.** Human adipose tissue stromal vascular cells were obtained from Boston Nutrition Obesity Research Center (BNORC). Briefly, abdominal subcutaneous adipose tissue were obtained during elective surgeries from human subjects [BMI, 40.5 ± 1.6 kg/m<sup>2</sup> (range 23-63); 41.4 ± 2.0 years (range 25-71) old; 33F, 6M; 11AA, 12H, 17C] who were free of diabetes, cancers, endocrine or inflammatory diseases by medical history. Surgeries took place at the Boston Medical Center. All subjects provided informed consents as approved by Institutional Review Boards of the Boston Medical Center. Adipose tissues were placed in type 1 collagenase (1 mg/ml in Hanks' balanced salt solution) for 2 h (22), and then the hADSCs within them were isolated by filtering with a 250- $\mu$ m mesh and centrifugation twice at 500  $\times$ g for 10 min. Between the centrifugation rounds, cell pellets were treated with erythrocyte lysis buffer [0.154 mM NH<sub>4</sub>Cl, 10 mM K<sub>2</sub>HPO<sub>4</sub>, and 0.1 mM ethylenediaminetetraacetic acid (EDTA), pH 7.3]. The re-pelleted cells were re-suspended in growth media ( $\alpha$ -Minimum Essential Medium-Alpha Eagle with 10% fetal bovine serum) and then plated for culturing. Cells were subcultured for up to six passages. CRISPR-Cas9 mediated KO cells were generated at passage 1 or 2. Cells from

individual subjects were used without pooling. Experiments were repeated in cells derived from at least three independent donors.

**Generation of T-brites.** Preadipocytes were plated in 12-well plates (5,000–15,000 cells/cm<sup>2</sup>) were cultured to confluency. Two day-post confluent cells were induced to differentiate in complete differentiation media (Dulbecco's Modification of Eagle's Medium/F12 with 500 μM IBMX, 100 nM insulin, 100 nM dexamethasone, 2 nM T3, 101 g/ml transferrin, 1 μM rosiglitazone, 33 μM biotin, and 17 μM pantothenic acid) for 7 d followed by maintenance in Dulbecco's Modification of Eagle's Medium F12 supplemented with 33 μM biotin, 17 μM pantothenic acid, 10 nM insulin, and 10 nM dexamethasone for 3 d. After complete maturation into white adipocytes, the cells were treated with 1 μM Rosi for 7 d to generate T-brites. Additionally, to induce britening mature white adipocytes were treated for 7 d with 1 nM CL316,243 (β3 agonist), 100 nM FGF21, or 100 nM ANP.

**DNA template engineering for in vitro transcription (IVT).** We generated Cas9 nickase by site directed mutagenesis of humanized WT spCas9. The resulting vectors were utilized to PCR amplify the Cas9D10A and Cas9H840A fragments. An all-in-one nickase multi-cistronic mRNA template containing a 2A-linked puromycin cassette, which expresses Cas9 nickase and puromycin from a single ORF, was generated; the 2A peptide sequence was sandwiched between the Cas9 nickase and puromycin frames (Fig. 1d). The puromycin cassette was amplified from pCW-Cas9 (Addgene #50665). The 2A peptide [(GSG) A T N F S L L K Q A G D V E E N P G P], 5'UTR, and 3'UTR of human beta-globin were synthesized as gBlocks. To append a T7 promoter in front of the 5'UTR, we PCR amplified the 5'UTR gBlock with a primer containing a T7 promoter. Next, to generate all-in-one Cas9 nickase, we assembled all the inserts in a single reaction with Gibson assembly master mix (E2611, New England BioLabs Inc.). Following

Gibson assembly, purified all-in-one Cas9 nickase product was PCR amplified with All-in-One F1 (forward primer containing T7 promoter) and All-in-One R1 (reverse primer containing 10-nt oligonucleotide dT tail with 10T to assist poly A tailing). All intermediate PCR and Gibson assembly products were purified with QIAquick spin columns (Qiagen, Valencia, CA). The oligonucleotide sequences used in template construction are shown in Supplementary Table 1. All oligonucleotides were synthesized by Integrated DNA Technologies (Coralville, IA)

To generate mod mRNA templates for *CIDEA*, *LXR $\alpha$* , *LXR $\beta$* , *RXR $\alpha$*  and *GAPDH*, the ORFs of these genes were human codon optimized (<https://www.idtdna.com/CodonOpt>) and synthesized as gBlocks. The ORFs were identical to the NCBI human transcript variants (*CIDEA*: NM\_001279.3, *LXR $\alpha$*  (NR1H3): NM\_005693.3, *LXR $\beta$* (NR1H2): NM\_007121.5, *RXR $\alpha$*  (*RXRA*): NM\_002957.5. In preliminary studies, 5'UTRs of AP2, beta-globin, *CIDEA*, and COL18A1 were appended to the GFP ORF along with the beta-globin 3'UTR. After examining the translation powers of GFP with different 5'UTRs through confocal microscopy, we chose the AP2 5'UTR for its high translational capacity in adipocytes. All UTRs were synthesized as gBlocks as described above.

To generate a 3 $\times$  HA or 6 $\times$ His tagged (N-terminus) *CIDEA* templates, AP2 5'UTR containing either tag sequence were synthesized as gBlocks. The AP2 5'UTR-3 $\times$ HA or AP2 5'UTR-6 $\times$ His were appended to the 5' end of the *CIDEA* ORF; the 3'UTR of beta-globin was appended simultaneously. The T7 promoter was appended in front of the 5'UTR. All sequences were assembled by Gibson assembly, as described above, and the purified products were PCR amplified with All-in-One F1 and All-in-One R1 primers (introduced above). Two NLS mutant *CIDEA*-HA constructs (*CIDEA*<sub>K23A</sub>-HA and *CIDEA*<sub>R44A</sub>-HA) were generated from a *CIDEA*

ORF by nested PCR with mutant primers. The mRNA templates for these two mutants were constructed as described above.

**Synthesis and purification of mod mRNA.** Purified construct templates (0.1–4 µg) were produced by IVT with a MEGAscriptT7 kit (Ambion, Austin, TX, USA) in 50-µl IVT reaction mixtures containing, at a molar ratio of 1:1:1:0.2:0.7, the following constituents: (1) 7.5 mM ATP; (2) 7.5 mM 5-methylcytidine-5'triphosphate; (3) 7.5 mM pseudouridine triphosphate/2-thiouridine-5'-triphosphate; (4) 1.5 mM GTP; and (5) 5 mM for the cap analog (#1–4 from TriLink BioTechnologies, San Diego, CA; #5 from New England Biolabs, Ipswich, MA). After IVT, mRNAs were polyadenylated (150~200 residues) using a poly(A) kit (Ambion). The IVT products were treated with Antarctic phosphatase (New England Biolabs) and the capped mRNAs that remained were purified with a MEGAclean kit (Ambion). The size and integrity of the mRNA products were verified by denaturing agarose gel electrophoresis.

**Mod mRNA transfection.** IVT mRNA was complexed to TransIT-mRNA (Mirus Bio, Madison, WI) according to the manufacturer's instructions in a reaction mixture containing 200 ng mRNA, 0.2 µl TransIT-mRNA reagent, and 0.15 µl Boost reagent in a final volume of 25 µl Opti-MEM (Invitrogen) medium (reagent quantities increased proportionately as needed). The mixture was incubated for 30 min before cell transfection.

**Generation of hUCP1 Promoter-Enhancer reporter constructs and luciferase assay.** To clone the human *UCP1* promoter-enhancer region, we designed *UCP1* promoter-enhancer-specific primers to amplify a 6.0-kb genomic region upstream of the human *UCP1* transcription start site (-6000 bp). The PCR product (6000 bp) was isolated from an agarose gel with a gel extraction kit (Qiagen) and cloned into a pGL3-basic vector. Several deletion constructs were

generated from PCR amplification (-4000 +1, -2800 +1, -1800 +1, -4000 -2800, -3800 -2800, -4000 -3850; primers in Supplementary Table 1) and cloned into the pGL3-basic vector. The  $\Delta$ 150bp deletion clone was generated by Gibson assembly of two overlapping PCR fragments [-6000 -4000 (2 kb) and -3850 +1 (3.850 kb)] and then cloned into a pGL3 basic vector. Multiple constructs containing DR1 and/or DR4 loss- and gain-of-function mutants (DR1- $\Delta$ DR4 = 134 bp, DR4- $\Delta$ DR1 = 137 bp, DR4 - 3XDR1 = 178bp, and 3XDR4-DR1 = 184 bp) were designed and synthesized as gBlock gene fragments (Invitrogen) and then cloned into pGL3-LUC vectors. pGL3-LUC vectors were then reverse transfected into differentiated human brite adipocytes with 2  $\mu$ l/ $\mu$ g DNA of lipofectamine 2000 (Invitrogen) according to the manufacturer's instructions, and then 48 h later, the cells were transfected with mod mRNAs [*GAPDH* (control), *CIDEA*, *LXR $\alpha$* , *LXR $\beta$* , and *RXR $\alpha$* ]. After 24 h of mod mRNA treatment, cells were treated with isoproterenol, Rosi, and T09 (only when *LXR $\alpha/\beta$*  was exogenously expressed) in the adipocyte maintenance media. The cells were harvested 12 h later and their luciferase activities were measured with a Promega Dual-Glo Luciferase Assay System. Values were normalized relative to the Renilla signal to allow for differences in transfection efficiency.

***In vitro* DNA pull-down assay in a cell-free system.** DNA pull-down assays were performed based on a previously described protocol (Deng et al. (2003) *Anal Biochem* 323, 12-18). Briefly, the 150-bp distal hUCP1 promoter region was amplified from human genomic DNA by PCR (Applied Biosystems) with biotinylated primers (Integrated DNA technologies; Supplementary Table 1) and platinum Green Master Mix (Invitrogen) under the following conditions: 94 °C for 5 min, forty 45-s 94-°C cycles, 58 °C for 30 s, 72 °C for 90 s, and 72 °C for 10 min. Additionally, 20-mer biotinylated and non-biotinylated (competing) DR1 and DR4 oligonucleotides corresponding to the 150-bp distal hUCP1 enhancer were synthesized

(Integrated DNA Technologies). *In vitro* translated proteins (hCIDEA, hLXR $\alpha$ , hRXR $\alpha$ , and hPPAR $\gamma$ ; 10  $\mu$ g each) were preconditioned with streptavidin magnetic beads (Dynabeads M270, Thermo-Fisher) for 30 min at 4 °C, and then incubated with 2  $\mu$ g biotinylated double-stranded DNA or 500 pmol biotinylated/non-biotinylated oligonucleotides overnight at 4 °C in a rotating shaker. The next day, DNA-protein-streptavidin-magnetic bead complexes were pulled down by magnetic stands for 5 min. The supernatants was discarded and the complexes were washed twice with cold Tris buffered saline (TBS). The beads were re-suspended in 25  $\mu$ l of 2 $\times$  sodium dodecyl sulfate (SDS) buffer, boiled at 95 °C for 5 min, and then the proteins were separated by SDS-polyacrylamide gel electrophoresis (PAGE) followed by western blotting with indicated antibodies. Non-biotinylated (competing) oligonucleotides were used as a control as well as to compare the strength of their biotinylated counterparts.

For *in vitro* crosslinking of the CIDEA-LXR $\alpha$  complex with DR4 followed by streptavidin-biotin pull down, short-arm (HCHO) and long-arm (EGS) crosslinkers were utilized (Zeng et al. (2006) *Biotechniques* 41, 694, 696, 698). The DNA-protein-streptavidin magnetic bead complexes were incubated with either 1% HCHO for 15 min alone or in 1.5 mM EGS for 30 min and then in 1% HCHO for 15 min. The crosslinking reaction was stopped with 50 mM glycine-PBS for 10 min, and the crosslinked mixture was centrifuged at 300  $\times$ g for 2 min followed by washing, as described above.

***In vitro* DNA pull-down assay.** Adipocyte nuclear extraction was performed with NE-PER™ nuclear and cytoplasmic extraction reagents (Thermo-Fisher) according to the manufacturer's protocol. Following nuclear extraction, 500  $\mu$ g of lysate was incubated with 5  $\mu$ g biotinylated DNA probes and 200  $\mu$ l streptavidin magnetic beads. The final volume was adjusted to 500  $\mu$ l with NER buffer from the kit. The mixture was placed on a rotating shaker and incubated

overnight at 4 °C. The samples were placed on a magnetic stand, washed with ice cold PBS three times, and washed once with NER buffer.

**ChIP assays.** ChIP assays were performed with a ChIP-IT assay kit (Active Motif, Carlsbad, CA) according to the manufacturer's instructions. Briefly, 1% HCHO-fixed chromatin was isolated from T-brites following glycine quenching. After sonication shearing of chromatin, crosslinked protein-DNA complexes were pre-cleared with protein-G-agarose and incubated with protein G-coated magnetic beads bound with LXR $\alpha$ . Complexes were precipitated with magnetic beads and the DNA was released, purified, treated with protease, and finally analyzed by real-time PCR with appropriate primers (Supplementary Table 1). Controls included anti-RNAPol II (positive), mouse IgG (negative), and non-reactive anti-GAPDH (negative) for immunoprecipitations and a set of random oligonucleotides for control PCR.

**IVTT and DNA template construction.** IVTT constructs were generated following the guidelines of Pierce's PCR protocol for generating optimized templates (TR0072.1). A 600-bp T7-IRES-Kozak sequence containing a T7 promoter, internal ribosome entry site, and Kozak sequence were amplified from pT7CFE1 vectors (no. 88860) with T7 sense and Kozak anti-sense primers. Next, an overlap sense primer (overlap with Kozak sequence) and an overlap anti-sense primer (overlap with gene ORF or fragments) containing a 30-nt poly-A sequence were utilized to amplify the gene ORF (*CIDEA*, *LXR $\alpha$* , *RXR $\alpha$* , or *PPAR $\gamma$* ) or gene fragment (*CIDEA*<sub>1-70aa</sub>, *CIDEA*<sub>33-110</sub>, *CIDEA*<sub>1-160aa</sub>, *CIDEA*<sub>71-160aa</sub>, *CIDEA*<sub>160-219aa</sub>, *CIDEA*<sub>70-184aa</sub>, *CIDEA*<sub>184-219aa</sub>, *CIDEA*<sub>1-219 $\Delta$ aa</sub>, *LXR $\alpha$* <sub>1-96aa</sub>, *LXR $\alpha$* <sub>97-200aa</sub>, *LXR $\alpha$* <sub>205-447aa</sub>, or *LXR $\alpha$* <sub>215-434aa</sub>). These two fragments were combined for overlap extension PCR with T7 sense and overlap anti-sense primers. PCR cycles were performed according to the guidelines. The resulting PCR templates were purified, and the identities of the templates were confirmed by restriction enzyme analysis; 1  $\mu$ g of template DNA

was utilized for 50 µl of transcription-translation reaction mixture with a 1-Step Human Coupled IVT Kit according to manufacturer's recommendations (Thermo-Scientific). A sample without added DNA was used as a negative control; GFP template DNA was used as a positive control. Translation reaction time was optimized for protein length to reduce truncated proteins due to material exhaustion. The reaction times were as follows: 1–100 aa = 360 min, 101–200 aa = 240 min, 201–300 aa = 180 min, 301–500 aa = 120 min, >501 aa = 90 min. Following translation, total protein concentration was calculated and small portions were subjected to western blotting to confirm protein integrity or placed in -80 °C storage for co-IP.

***In vitro* CRISPR-Cas9D10A DNA cleavage assay in a cell-free system.** To test the *in vitro* efficacy of the CRISPR/hCas9D10A system, we used IVTT synthesized hCas9D10A protein. This Cas9 protein (1 µg) was incubated with each gRNA (50 nM) and the PCR amplified human *CIDEA* sequence (500 ng) containing all exons. This reaction was performed in 1×NEB buffer 3 with 1×NEB BSA at 37 °C for 1 h. Following treatment with RNase (Invitrogen) and 0.5 µl proteinase K (molecular biology grade, New England Biolabs) for 15 min at 37 °C, *CIDEA* DNA fragments resulting from CRISPR/hCas9D10A-induced cleavage were analyzed by agarose gel electrophoresis.

**T7E1 assay.** We extracted genomic DNA from cells 3 d after nucleofection using a DNA isolation kit for cells and tissues (Sigma-Aldrich) following the manufacturer's instructions. PCR amplicons spanning the sgRNA genomic target sites (*CIDEA* exon 4) were generated with Platinum Hot Start PCR Master Mix (2×)(Thermo-Fisher) with the indicated primer pairs. PCR amplicons were purified, from which 250 ng was denatured, re-annealed in a thermocycler, and digested with T7E1 (New England Biolabs, Waltham, MA) in accordance with the manufacturer's protocol. Digested DNA was run on a 5% TBE polyacrylamide gels, stained with

ethidium bromide solution (Sigma-Aldrich), and visualized on a ChemiDoc (Bio-Rad). Band intensities were analyzed with Image Lab Software (Bio-Rad) and allele modification frequencies were calculated as follows:  $100 \times [1 - (1 - \text{fraction cleaved})^{0.5}]$ .

**CRISPR/Cas9 Nickase mutagenesis.** Freshly isolated hADsc were plated in 10cm dish. At passage 1 the confluent cells (~80%) were forward and reverse transfected with 5-30  $\mu\text{g}$  of hspCas-D10A mod RNA. After 12 hrs of transfection, puromycin (1.5  $\mu\text{g}/\text{ml}$ ) was added in the culture media to create a positive selection pressure. Additionally, after 48hrs of Cas9 nickase mod mRNA transfection, modified sgRNA pair (1 & 2) was reverse transfected. The transfection mixture also contained AZT (5  $\mu\text{M}$  concentration) (Azidothymidine, sigma) a small molecular CRISPR indel enhancer. After another 72hrs of puromycin selection (0.5  $\mu\text{g}/\text{ml}$ ), the remaining cells were trypsinized and re-plated in 12 wells plates at a seeding density of  $1 \times 10^4$  cells/well with equivalent mixture of pre-adipocyte GM and pre-adipocyte conditioned media. This media was supplemented with rho associated protein kinase inhibitor Y-27632 to increase the clonal population. After 5 days of expansion, cells were harvested to isolate genomic DNA for T7 E1 assay. CIDEA transcript and protein was completely absent in preadipocytes. Therefore, to check the loss of function of CIDEA, we induced CIDEA transcription in these nonconfluent preadipocytes by 12 hr incubation in adipocyte differentiation media, containing 0.1  $\mu\text{M}$  Rosi. To measure the loss of function, we designed five sets of real time primers targeting each exon or exon intron boundary. Of two primers targeting CIDEA exon 4, one primer was designed to locate between two sgRNA. It is expected that Cas9 Nickase mediate indel would not interfere with another exons transcription.

***In situ* protein-protein interaction PLA.** The mouse/rabbit red starter Duolink kit (DUO92101, Sigma-Aldrich) was used according to the manufacturer's protocol. Briefly, Rosi-induced,

terminally-differentiated human WT (CIDEA<sup>+/+</sup>) or KO (CIDEA<sup>-/-</sup>) T-brites were cultured on lysine-coated coverslips (Sigma-Aldrich), fixed with 4% paraformaldehyde for 15 min, and quenched with 2% glycine for 15 min. Next, cells were permeabilized with 0.025% Triton-x in TBS with 0.1% Tween 20 (TBST), blocked for 1 h, and then incubated with the indicated primary antibodies overnight in TBST. Cells incubated with primary antibodies only or with/without PLA probes only (mouse and rabbit) were assay controls. The cells were then incubated with oligonucleotide-conjugated PLA probes for 60 min followed by ligation of PLA probes in a preheated humidified chamber for 30 min at 37 °C. The signal was amplified for 100 min in same humidified chamber and visualized under a Nikon confocal microscope.

**Immunofluorescence and western blotting.** Confocal microscopy was performed with a Zeiss LSM 710-Live Duo scan (Carl Zeiss, Oberkochen, Germany) or Nikon A1R (Nikon, Japan) with a 60× or 100× oil immersion objective. For immunofluorescence, hADSCs that had been differentiated into T-brites on poly-L-lysine coated glass cover slips in 24-well plates and transfected (24 h before sample preparation) with TransIT-mRNA (Mirus Bio, Madison, WI) were fixed with 4% para-formaldehyde (10 min), and then placed, in series, in 2% glycine (10 min), 0.025% Triton X-100 (5 min), PBST (3 times for washing), 10% goat serum B (10 min), and primary antibodies in TBST with 4% goat serum (overnight, 4 °C). Coverslips were washed three times with PBST and incubated for 2 h in the dark with secondary antibodies (Alexa Fluor 488 or 594, in PBST with 4% goat serum). Cells on coverslips were washed three times with PBST before LD staining with HCS LipidTOX-Deep Red or HCS LipidTOX Red (Invitrogen) for 20 min. Finally, the cells were washed with PBS three times before mounting on glass slides with Vecta Shield media (Vector Labs, CA) with or without 4',6-diamidino-2'-phenylindole

dihydrochloride nuclear counterstain. Images were processed with ImageJ and Adobe Photoshop®.

For western blotting, cells were lysed in 1× lysis buffer (Roche) supplemented with phosphatase and protease inhibitors (1 µg/ml aprotinin, 1 µg/ml pepstatin, 1 µg/ml leupeptin, 1 mM phenylmethane sulfonyl fluoride, and 1 µg/ml trypsin inhibitor) and 1% Triton X-100, followed by sonication and incubation on ice for 2 h. Subsequently, the cells were centrifuged at 7,500 rpm for 30 min at 4 °C. The supernatants were collected and protein quantities was estimated by the Bradford method; 25–50-µg total protein aliquots from each sample were resolved by 10–12% SDS-PAGE.

**Mitochondrial DNA copy number and total oxidative phosphorylation protein analysis.** To quantify mitochondrial DNA in WT and KO T-brites, total cellular mitochondria were isolated with an Abcam mitochondrial isolation kit (ab110171) according to the manufacturer's instructions. Mitochondrial DNA copy number was quantified with primers specific for the mitochondrial D-loop region and nuclear genome specific  $\beta$ 2 microglobulin by quantitative PCR. The mtDNA copy number/cell is represented by the D-loop:nuclear target ratio.

For oxidative phosphorylation protein analysis, 20 µg of mitochondria was denatured in SDS sample buffer for 5 min at 50 °C and then separated in 4–12% Bis/Tris gels (3-morpholinopropane-1-sulfonic acid buffer). Transfer membranes were blocked in 4% BSA-TBST for 4 h at room temperature, and then incubated with a primary antibody cocktail (1:1000; Abcam, ab110411) for 4 h at room temperature. After three washes with TBST, the membranes were incubated with horseradish peroxidase-conjugated goat-anti-mouse secondary antibody

(1:10000) for 1 h at room temperature. Peroxide activity was visualized by enhanced chemiluminescence and exposure to x-ray film.

**UCP1 promoter- enhancer analysis and CIDEA NLS prediction.** The human UCP1 promoter- enhancer sequence was downloaded from the UCSE browser and confirmed to be a strong match for the human sequence in ENSEMBL. A transcription start site was annotated in a CpG island-rich region. Multiple putative LXREs were identified in the vicinity of a primate-specific Alu element in both strands. Binding efficiencies were calculated based on the most conserved consensus DR4-LXRE motif (ACGTCA-TAAA-GGGTCA). A binding strength  $\geq 0.5$  was considered strong. We aligned orthologous human and mouse *UCP1* promoter sequences in CLUSTALW and determined the maximum conservation score around LXRE/RXR. We utilized several programs to analyze the promoters: <http://cisreg.cmmt.ubc.ca/cgi-bin/tfe/home.pl>; <http://www.cisreg.ca/cgi-bin/mscan/MSCAN>; [github.com/amathelier/DNAshapedTFBS](https://github.com/amathelier/DNAshapedTFBS); [http://algggen.lsi.upc.es/cgi-bin/promo\\_v3/promo/promoinit.cgi?dirDB=TF\\_8.3](http://algggen.lsi.upc.es/cgi-bin/promo_v3/promo/promoinit.cgi?dirDB=TF_8.3); and <http://opossum.cisreg.ca/oPOSSUM3/>. We used SeqNLS (lin and Hu (2013) PLoS One 8, e76864), cNLS Mapper (lin and Hu (2013) PLoS One 8, e76864), and NucPred (Brameier et al. (2007) Bioinformatics 23, 1159-1160) for NLS prediction of the human CIDEA protein sequence (NP\_001270.1).

**Cycloheximide and FFA mixture chase assay.** Following a 6-h incubation in ISO, mature T-brites were subjected to chase assays with 30  $\mu\text{g}/\text{mL}$  CHX or 5% FFAs and then harvested immediately or 3 h, 6 h, 18 h after treatment. Nucleus/LD fractions isolated by subcellular fractionation (described above) were subjected to western blotting with indicated antibodies.

**Quantification of gene expression by real time PCR.** Total RNA was isolated from differentiated adipocytes with TRIzol and cDNAs were synthesized with a M-MuLV reverse transcriptase kit (MBI Fermentas, USA). Real-time PCR was performed with Power SYBR green dye in a Step One Plus Real Time PCR System (Applied Biosystems, Foster City, CA) according to the following program: 95 °C for 10 min, 35 15-s cycles at 95°C, 55–61°C for 30 s, 72 °C for 30 s, and a final melting curve step. The collected CT values were normalized to an internal control, peptidylprolyl isomerase. There were five determinations using five individual experiments. The results (mean ± standard errors) were expressed as fold changes relative to the same gene in control human differentiated adipocytes.

**Seahorse bioenergetic analysis.** Approximately 15,000 hADSCs at passage 4 were seeded in 100 µl media/well of an XF24 V7 plate for OCR measurement at 37 °C by an XF24 analyzer (Seahorse Bioscience). On day 8 of differentiation, 2 h before OCR measurement, human britening media was replaced with pre-warmed Seahorse XF assay medium (supplemented with 20 mM glucose, 1 mM Na-pyruvate, 2 mM GlutaMax, 0.8 mM Mg<sup>2+</sup>, 1.8 mM Ca<sup>2+</sup>, 143 mM NaCl, 5.4 mM KCl, 0.91 mM NaH<sub>2</sub>PO<sub>4</sub>, and 15 mg/l phenol red, pH 7.4) and incubated at 37 °C in an air incubator (without CO<sub>2</sub>) for 45–60 min. Mitochondrial assay compounds were loaded into injection ports (50 µl/port) and four assay cycles (cycle: 1 min mix, 3 min wait, 3 min measuring period) were used to determine basal respiration, and then ATP coupled respiration was inhibited by 5 µM oligomycin. Maximum respiratory capacity was assessed after addition of 1 mM FCCP (Tocris). Finally, mitochondrial respiration was blocked by injection of a 1:1 mixture of rotenone and antimycin A (5 µm each; Tocris) to correct for non-mitochondrial respiration rate. FCCP was injected with Na-pyruvate (10 mM); other compounds were injected with assay medium. ISO (1 µM) was injected to measure the contribution of UCP1 mediated

uncoupled respiration. For some experiments, cells were pretreated with orlistat (50  $\mu\text{M}$ ) or CSA (5  $\mu\text{g/ml}$ ) for 1 h in human browning media. Both were present at same concentration in the assay medium during ISO mediated stimulation. In a separate experiment, TTNPB (0  $\mu\text{M}$ , 5  $\mu\text{M}$ , 10  $\mu\text{M}$ , 25  $\mu\text{M}$ , 50  $\mu\text{M}$ , and 100  $\mu\text{M}$  in DMSO) or nonanoic acid (0  $\mu\text{M}$ , 5  $\mu\text{M}$ , 10  $\mu\text{M}$ , 25  $\mu\text{M}$ , 50  $\mu\text{M}$ , and 100  $\mu\text{M}$ ) was injected with assay medium to determine the effective TTNPB concentration. OCRs were calculated in Seahorse XF-96 software. Data were exported and reconstructed in GraphPad Prism 5.0 software. After completion of each assay, proteins were isolated from each well for UCP1 expression FABP4 expression determination. Each experiment was repeated 3–5 times with similar results.

**Cellular import assay.** *In vitro* nuclear transport assays were conducted as previously described (Wagstaff et al. (2012) *Biochem J* 443, 851-856; Whitehurst et al. (2002) *Proc Natl Acad Sci U S A* 99, 7496-7501) with minor modifications. For analysis of the influence of Imp $\alpha/\beta$  on CIDEA import, we treated T-brites with 5  $\mu\text{M}$  of ivermectin (Sigma) at the same time as CIDEA-HA and SV40-T-Ag-HA mRNA transfection. Cells were fixed and subjected to immunofluorescence 24 h later. To check whether CIDEA import depends on active transport, T-brites on coverslips were washed with import buffer (20 mM HEPES, 110 mM potassium acetate, 2 mM magnesium acetate, 1 mM EGTA, and 2 mM dithiothreitol). To deplete cellular internal transport factors, cells were permeabilized with digitonin (50  $\mu\text{g/ml}$ ; Sigma) in import buffer for 5 min on ice. For the energy-dependence experiments, an energy regenerating transport mixture (50  $\mu\text{l/cover slip}$ ) was prepared by mixing 25  $\mu\text{l}$  rabbit reticulocyte lysate (Promega) with 25  $\mu\text{l}$  import buffer containing 1 mM ATP, 0.1 mM GTP, 5 mM creatine phosphate, and a protease inhibitor mix (source or recipe). To measure the energy-dependent import of substrates (CIDEA and SV40-T-Ag), CIDEA-HA, and T-Ag-HA were translated *in vitro* as described above. The substrates were

added to a final concentration of 5  $\mu\text{g}/50 \mu\text{l}$  in the transport mixture and then 50  $\mu\text{l}$  of the transport mixture was added drop-wise to cover each whole coverslip, and the mixture was incubated in a cell culture incubator for 60 min. The cells were washed, fixed with 4% paraformaldehyde, and subjected to immunofluorescence with anti-HA primary antibody. To generate an energy depleted import mixture, rabbit reticulocyte lysates were pretreated with apyrase (25 U/ml, New England Biolabs) at 30 °C for 30 min before adding the import mixture (also ATP-, GTP-, and creatine phosphate-free) to the cells.

**Quantification of protein-DNA interaction strength with the modified restriction fragment length polymorphism (RFLP) method.** We used the dUER<sub>150bp</sub> (i.e., 150-bp UCP1 distal enhancer region containing DR1 and DR4) sequence as target DNA, with a unique AatII restriction site (GACGT\*C/C\*TGCAG) created by site directed mutagenesis (T>A) near the DR4 sequence by nested PCR with mutant primers (Supplementary Table 1). Target DNA (500 ng) was incubated at 37 °C for 30 min in reaction buffer (1 $\times$  NEB 1 $\times$  CutSmart® buffer) with *in vitro* translated LXR $\alpha$  and RXR $\alpha$  (5  $\mu\text{g}$  each) in a final volume of 50  $\mu\text{l}$ . Following incubation with LXR $\alpha$ , *in vitro* translated CIDEA or BSA (1–5  $\mu\text{g}$ ) was added to the reaction mixture, which was then incubated at 37 °C for an additional 30 min. The post-CIDEA reaction mixture was incubated with 5 U of AatII restriction enzyme at 37 °C for 45 min. The digested DNA was resolved in a 2.5% agarose gel and visualized by DNA staining. Cleavage efficiency was determined as the intensity ratio of cleaved to uncleaved bands in ImageJ. The  $\Delta\text{DR4}$  150-bp target cleavage and 150-bp target cleavage in the presence of BSA were utilized as controls. The strength of AatII-mediated LXR $\alpha$  bound DR4 cleavage is directly proportional to the amount of CIDEA in the reaction.

